

**MODELING COMBUSTION OF MULTICOMPONENT FUEL DROPLETS:  
FORMULATION AND APPLICATION TO TRANSPORTATION FUELS**

A Thesis

by

KANNAN VITILAPURAM SUBRAMANIAN

Submitted to the Office of Graduate Studies of  
Texas A&M University  
in partial fulfillment of the requirements for the degree of

MASTER OF SCIENCE

December 2004

Major Subject: Mechanical Engineering

**MODELING COMBUSTION OF MULTICOMPONENT FUEL DROPLETS:  
FORMULATION AND APPLICATION TO TRANSPORTATION FUELS**

A Thesis

by

KANNAN VITILAPURAM SUBRAMANIAN

Submitted to Texas A&M University  
in partial fulfillment of the requirements  
for the degree of

MASTER OF SCIENCE

Approved as to style and content by:

---

Kalyan Annamalai  
(Chair of Committee)

---

Jerald Caton  
(Member)

---

Yassin Hassan  
(Member)

---

Dennis O'Neal  
(Head of Department)

December 2004

Major Subject: Mechanical Engineering

## ABSTRACT

Modeling Combustion of Multicomponent Fuel Droplets: Formulation and Application to  
Transportation Fuels. (December 2004)

Kannan Vittilapuram Subramanian, B.En. and M.S., Birla Institute of Technology and Science,  
Pilani

Chair of Advisory Committee: Dr. Kalyan Annamalai

The quasi-steady, spherically symmetric combustion of multicomponent isolated fuel droplets has been modeled using modified Shvab-Zeldovich variable mechanism. Newly developed modified Shvab-Zeldovich equations have been used to describe the gas phase reactions. Vapor-liquid equilibrium model has been applied to describe the phase change at the droplet surface. Constant gas phase specific heats are assumed. The liquid phase is assumed to be of uniform composition and temperature. Radiative heat transfer between the droplet and surroundings is neglected.

The results of evaporation of gasoline with discrete composition of hydrocarbons have been presented. The evaporation rates seem to follow the pattern of volatility differentials. The evaporation rate constant was obtained as  $0.344\text{mm}^2/\text{sec}$  which compared well with the unsteady results of Reitz et al. The total evaporation time of the droplet at an ambience of  $1000\text{K}$  was estimated to be around 0.63 seconds. Next, the results of evaporation of representative diesel fuels have been compared with previously reported experimental data. The previous experiments showed sufficient liquid phase diffusional resistance in the droplet. Numerical results are consistent with the qualitative behavior of the experiments. The quantitative deviation during the vaporization process can be attributed to the diffusion time inside the droplet which is unaccounted for in the model. Transient evaporation results have also been presented for the

representative diesel droplets. The droplet temperature profile indicates that the droplet temperature does not reach an instantaneous steady state as in the case of single-component evaporation.

To perform similar combustion calculations for multicomponent fuel droplets, no simple model existed prior to this work. Accordingly, a new simplified approximate mechanism for multicomponent combustion of fuel droplets has been developed and validated against several independent data sets. The new mechanism is simple enough to be used for computational studies of multicomponent droplets.

The new modified Shvab-Zeldovich mechanism for multicomponent droplet combustion has been used to model the combustion characteristics of a binary alcohol-alkane droplet and validated against experimental data. Burn rate for the binary droplet of octanol-undecane was estimated to be  $1.17\text{mm}^2/\text{sec}$  in good concurrence with the experimental value of  $0.952\text{mm}^2/\text{sec}$  obtained by Law and Law. The model has then been used to evaluate the combustion characteristics of diesel fuels assuming only gas phase reactions. Flame sheet approximation has been invoked in the formulation of the model.

**TO  
MY PARENTS**

## ACKNOWLEDGEMENTS

The following paragraphs mean more to me than what may be judged on the basis of contribution. I believe it to be the culmination of a noteworthy chapter in my life so far, which I'm sure would continue to defy all physical laws in taking the many strange ups and downs and turns. This experience would not have been possible without the contribution of many, who directly or indirectly made it enjoyable and doable.

To begin with, I would like to thank my thesis advisor, Dr. Kalyan Annamalai. Much of the work presented in this thesis has been the culmination of the ideas that he continuously provided. My contributions are clearly the result of his allowing me to independently explore and conduct my work.

I am very grateful to Dr. Jerald Caton for offering guidance throughout and for being extremely helpful. My words would not be complete without the mention of my lab mates, Soyuz and Senthil, with whom I've shared many light and serious moments.

My stay at A&M would not have been enjoyable without the many personal friendships I have developed. My roomies (Arun, Anish, Praveen), and others (Kast, Vinod, Bullet, Lavanya, Ramya to name a few) have always been a constant source of support. Besides combustion, I got to learn about life, religion and politics from them.

Finally, I'm forever indebted to my mother and father, brother and other family members for the impact they have had on my life.

## NOMENCLATURE

### *Dimensional Parameters*

$a$	radius of droplet (m)
$c_p$	specific heat at constant pressure ( $\text{kJ kg}^{-1} \text{K}^{-1}$ )
$D$	diffusion coefficient ( $\text{m}^2 \text{s}^{-1}$ )
$h_c$	enthalpy of combustion ( $\text{kJ kg}^{-1}$ )
$h_t$	thermal enthalpy ( $\text{kJ kg}^{-1}$ )
$\alpha$	evaporation/burning rate constant, $-d(d_s^2)/dt$
$L$	enthalpy of vaporization ( $\text{kJ kg}^{-1}$ )
$m$	mass evaporation/burn rate ( $\text{kg s}^{-1}$ )
$p$	partial pressure (bar)
$P$	absolute pressure (bar)
$\dot{q}$	chemical heat generation rate ( $\text{kJ m}^{-3}$ )
$r$	radial distance (m)
$R$	universal gas constant ( $\text{kJ kg}^{-1} \text{K}^{-1}$ )
$T$	temperature (K)
$\vec{v}$	species bulk velocity ( $\text{m s}^{-1}$ )
$\dot{w}'''$	chemical production rate ( $\text{kg m}^{-3}$ )
$W$	molecular weight ( $\text{kg kmol}^{-1}$ )

### *Dimensionless Parameters*

$B$	transfer number
$H$	heat input function

s	$\frac{Y_{o,\infty}}{v_{o_2,avg}}$
X	mole fraction
Y	mass fraction
$v_{o_2}$	stoichiometric oxidizer to fuel mass ratio
$v_{o_2,avg}$	$\sum v_{o_2,i} \mathcal{E}_i$

### *Greek Symbols*

$\beta$	SZ variable
$\nabla$	differential operator
$\varepsilon$	flux ratio
$\lambda$	thermal conductivity ( $\text{kJ m}^{-1} \text{K}^{-1}$ )
$\rho$	density ( $\text{kg m}^{-3}$ )
$\xi$	rate of evaporation

### *Subscripts*

avg	average conditions
A	component A
bp	boiling condition
B	component B
comb	combustion
evap	evaporation
f	flame
F	fuel species
g	gaseous phase



i	$i^{\text{th}}$ component
iso	isolated
I	inert species
l	liquid phase
multi	multiple component
N	total number of species
o	oxidizer species
sat	saturation
w	interface conditions at droplet wall
$\infty$	ambient conditions

## TABLE OF CONTENTS

	Page
ABSTRACT.....	iii
DEDICATION.....	v
ACKNOWLEDGEMENTS.....	vi
NOMENCLATURE.....	vii
TABLE OF CONTENTS.....	x
LIST OF FIGURES.....	xii
LIST OF TABLES.....	xiv
1. INTRODUCTION.....	1
2. REVIEW OF LITERATURE.....	4
2.1 Droplet combustion theory.....	4
2.2 Multicomponent droplet combustion theory.....	15
2.3 Thesis organization.....	18
3. OBJECTIVE.....	20
4. THEORETICAL FORMULATION OF EVAPORATION AND COMBUSTION MODELS.....	21
4.1 Introduction.....	21
4.2 Droplet evaporation model.....	21
4.2.1 Gas phase.....	22
4.2.2 Vapor-liquid interface.....	25
4.3 Droplet combustion model.....	26
4.3.1 Assumptions.....	27
4.3.2 Gas phase.....	28
4.3.3 Interface boundary conditions.....	32
4.3.4 Phase change relations.....	33
4.3.5 Solutions.....	34
4.3.6. Liquid phase balance.....	35
5. RESULTS AND DISCUSSION.....	37
5.1 Introduction.....	37
5.2 Evaporation results.....	37
5.2.1 Gasoline droplet.....	37

	Page
5.2.2 Diesel droplet .....	44
5.2.3 Comparison with experimental results .....	52
5.3 Combustion results .....	55
5.3.1 Octanol-Undecane droplet .....	55
5.3.2 Diesel droplet .....	56
5.3.3 Comparison with experimental results .....	63
6. SUMMARY AND FUTURE WORK .....	65
6.1 Summary .....	65
6.1.1 Gasoline droplet evaporation results .....	65
6.1.2 Diesel droplet evaporation results .....	66
6.1.3 Octanol-Undecane droplet combustion results .....	66
6.1.4 Diesel droplet combustion results .....	67
6.2 Future work .....	68
6.2.1 Multicomponent experiments .....	68
6.2.2 Droplet combustion modeling .....	68
6.2.3 Study of droplet interior .....	69
REFERENCES .....	70
APPENDIX A .....	73
APPENDIX B .....	76
APPENDIX C .....	78
APPENDIX D .....	80
VITA .....	81

## LIST OF FIGURES

		Page
Figure 1.1	Energy consumption by fuel (quadrillion Btu's) from 1970-2025....	2
Figure 2.1	Schematic of spherically symmetric droplet combustion. ....	5
Figure 2.2	Schematic showing convective droplet combustion without flow separation. ....	6
Figure 2.3	Schematic showing convective droplet combustion with flow separation. ....	6
Figure 2.4	Schematic of classical $d^2$ -law single droplet combustion model.....	8
Figure 2.5	Droplet surface regression, flame standoff ratio and burn rate as a function of time as predicted by quasi steady formulation. ....	11
Figure 2.6	Actual observations indicating heat up time and flame standoff variations as a function of time. ....	12
Figure 2.7	Relaxation in $d^2$ -law assumption: Energy equation at interface accounting for droplet heat-up. ....	13
Figure 2.8	Relaxation in $d^2$ -law assumption: Vapor accumulation between flame and droplet.....	14
Figure 2.9	Profile of multicomponent fuel vapor species in gas phase assuming flame sheet combustion .....	16
Figure 5.1	Evaporation of stagnant gasoline droplet in quiescent ambient air... ..	41
Figure 5.2	Relative volatilities of components of gasoline droplet at different temperatures .....	42
Figure 5.3	Vaporization characteristics of individual species of gasoline droplet.....	43
Figure 5.4	Relative volatilities of components of diesel droplet at different temperatures.....	45
Figure 5.5	Temporal variation of volatile molar fractions for mixtures of hexadecane with tetradecane, dodecane and decane undergoing evaporation at 1020K.....	48
Figure 5.6	Temporal variation of diameter for mixtures of hexadecane with tetradecane, dodecane and decane undergoing vaporization at 1020K .....	49

	Page
Figure 5.7	Gas phase temperature profile for binary droplets of diesel undergoing vaporization at 1020K..... 50
Figure 5.8	Gas phase concentration profiles of binary droplet of hexadecane with tetradecane undergoing vaporization ..... 51
Figure 5.9	Gas phase concentration profiles of binary droplet of hexadecane with dodecane undergoing vaporization..... 51
Figure 5.10	Gas phase concentration profiles of binary droplet of hexadecane with decane undergoing vaporization..... 52
Figure 5.11	Temporal behavior of temperature of binary droplets of diesel undergoing unsteady vaporization..... 53
Figure 5.12	Temporal variation of volatile component mass fraction of diesel droplets undergoing unsteady vaporization ..... 54
Figure 5.13	Comparison of model and experimental burn rates of a binary droplet of octanol and undecane..... 57
Figure 5.14	Temporal variation of volatile molar fractions for mixtures of hexadecane with tetradecane, dodecane and decane undergoing combustion at 1300K..... 58
Figure 5.15	Temporal variation of diameter for mixtures of hexadecane with tetradecane, dodecane and decane undergoing combustion at 1300K. .... 60
Figure 5.16	Gas phase temperature profiles for binary droplets of diesel undergoing combustion ..... 61
Figure 5.17	Gas phase concentration profiles of oxygen, hexadecane and tetradecane for a binary droplet of hexadecane and tetradecane undergoing combustion..... 62
Figure 5.18	Gas phase concentration profiles of oxygen, hexadecane and dodecane for a binary droplet of hexadecane and dodecane undergoing combustion..... 62
Figure 5.19	Gas phase concentration profiles of oxygen, hexadecane and decane for a binary droplet of hexadecane and decane undergoing combustion..... 63

## LIST OF TABLES

		Page
Table 2.1	Assumptions incorporated in the formulation of $d^2$ -law for droplet combustion.....	9
Table 4.1	Values of $h_{c,o2}$ for some representative hydrocarbons found in gasoline and diesel .....	31
Table 5.1	Thermodynamic properties and composition of the components of gasoline.....	38
Table 5.2	Input data for isolated gasoline droplet evaporation.....	39
Table 5.3	Evaporation rates of the components of representative gasoline fuel vaporizing at $T_\infty=1000K$ , $P_\infty=1bar$ with $c_p=1.942kJ/kgK$ and $T_w=284K$ .....	40
Table 5.4	Thermo-physical properties of hydrocarbons representative of diesel fuels .....	44
Table 5.5	Table of input data for isolated diesel droplet evaporation.....	46
Table 5.6	Thermo-physical properties of octanol and n-undecane .....	55
Table 5.7	Calculated property values for the binary droplets representative of diesel fuels. ....	59

## 1. INTRODUCTION

The total energy consumption has been projected to increase annually at an average annual rate of 1.5% (Annual Energy Outlook<sup>1</sup>). Transportation energy demand has been projected to grow at an average annual rate of 2.0%. The higher level of consumption in the transportation sector results from the higher forecast of vehicle miles traveled and lower level of vehicle efficiency. Thus, despite efforts to utilize renewable energy resources, a majority of all energy consumed is derived from the combustion of fossil fuels. Fig. 1.1 indicates energy consumption by fuel with projections up to 2025. As we continue to rely on liquid petroleum based fuels as a major source of energy despite their finite supply, it is of great importance to maximize the efficiency of the devices which burn these fuels. The most effective way to achieve this goal is through a fundamental understanding of liquid vaporization and combustion processes. Vaporization and combustion of droplets and sprays has been an issue of much interest for decades because of its significance in engineering applications. Along with experimental studies, substantial effort has been made to predict the behavior of vaporizing droplets and sprays numerically.

In practical applications, liquid fuels are introduced into combustion devices as sprays of droplets. In most spark ignition engines, the sprays are vaporized and mixed with air prior to ignition. In other applications, such as diesel engines, jet engines and furnaces, combustion occurs next to the point of injection. The former case results in an essentially premixed flame while the latter results can result in flames varying from premixed, group and individual drop flame.

---

This thesis follows the style and format of the *Journal of the Institute of Energy*.

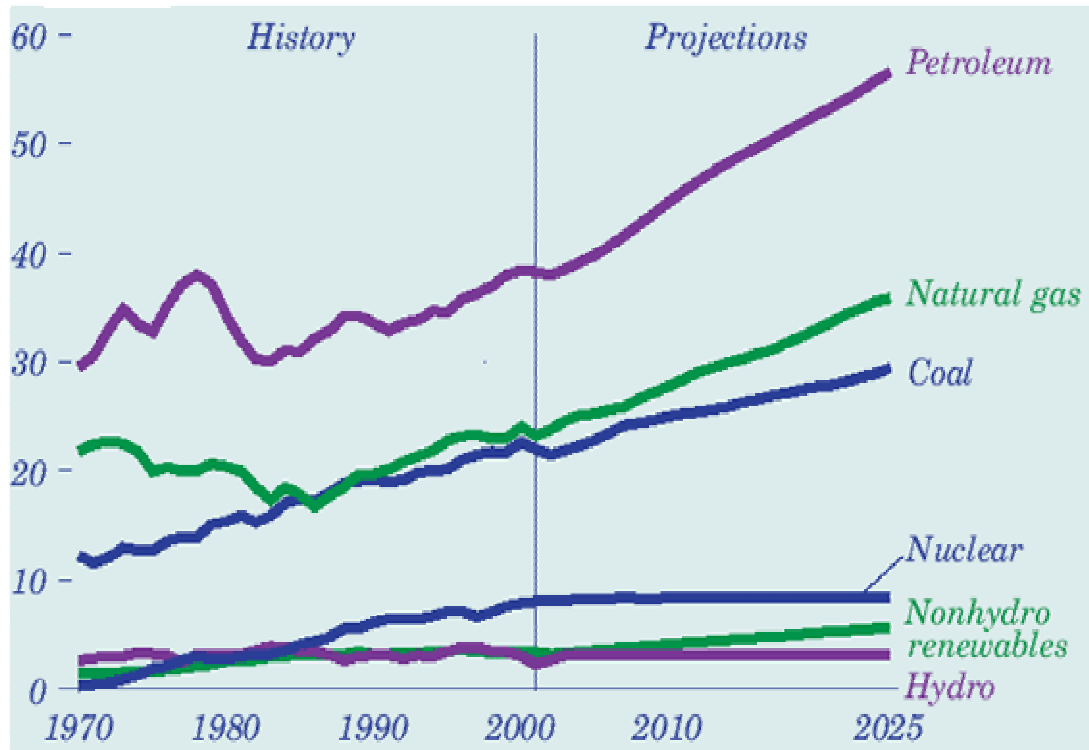


Fig. 1.1 Energy consumption by fuel (quadrillion Btu's) from 1970-2025 (Source: Annual Energy Outlook 2003, EIA).

In both cases, the underlying chemical, thermodynamic and transport processes are obscured by the complex, turbulent hydrodynamic environment inherent to these systems.

A simple experiment to fundamentally study the underlying physical phenomena of liquid spray combustion is to study the combustion of a single, isolated fuel droplet. In the simplified model, liquid phase transport of species, phase change, gas phase transport, gas phase chemical reaction and regression of the liquid surface are all present and coupled. Accordingly, the



combustion of isolated liquid droplet has served as the basis for much of the development of combustion theory.

In this thesis, the results of evaporation of gasoline and diesel fuels based on previously developed vaporization model of Annamalai *et al.*<sup>2</sup> and the formulation of an approximate combustion model for multicomponent droplets is presented. The model has then been validated and applied to representative diesel fuels. In the introductory section, brief reviews of droplet evaporation and combustion theory will be presented along with an organization of the new formulation and results, which will be presented in subsequent sections.

## 2. REVIEW OF LITERATURE

### 2.1 DROPLET COMBUSTION THEORY

Research on evaporation/gasification and combustion of fuel droplets commands both practical and fundamental interest to energy and combustion science. Hence, it is of paramount importance to study and understand the modes of droplet combustion. On the fundamental aspect, droplet combustion is a problem involving complex chemically reacting multicomponent mechanism with phase change, rich in physical and chemical phenomena.

Some possible droplet combustion modes (Sirignano and Law<sup>3</sup>) are shown in Figs. 2.1-2.3. In Fig. 2.1, the fuel droplet is motionless in a stagnant, gravity-free, oxidizing environment of infinite extent. The lack of either forced or natural convection implies the assumption of spherical symmetry. The basic mechanisms leading to the complete gasification of the droplet are heat and mass diffusion due to the existence of temperature and concentration gradients, the radial velocity convection because of the continuous transfer of mass from the droplet surface to the ambience, and chemical reaction in the flame region. The burning is of diffusion-flame type in which the outwardly diffusing fuel vapor and the inwardly diffusing oxidizer gas approach the reaction zone in approximate stoichiometric proportion. Reaction between fuel vapor and oxidant is rapid and intense, implying that the reaction zone is thin and very little reactants can leak through the flame. The heat generated at the flame is transported both outward and inward to heat up the approaching oxidizer and fuel gases in order to achieve ignition. The rest of the inwardly transported heat is used for droplet heating and to effect liquid gasification.

- |                                     |                       |
|-------------------------------------|-----------------------|
| ① Droplet                           | ⑤ Combustion Products |
| ② Inner Diffusive-Convective region | ⑥ Oxidizer gas        |
| ③ Outer Diffusive-Convective region | ⑦ Ambience            |
| ④ Fuel Vapor                        |                       |

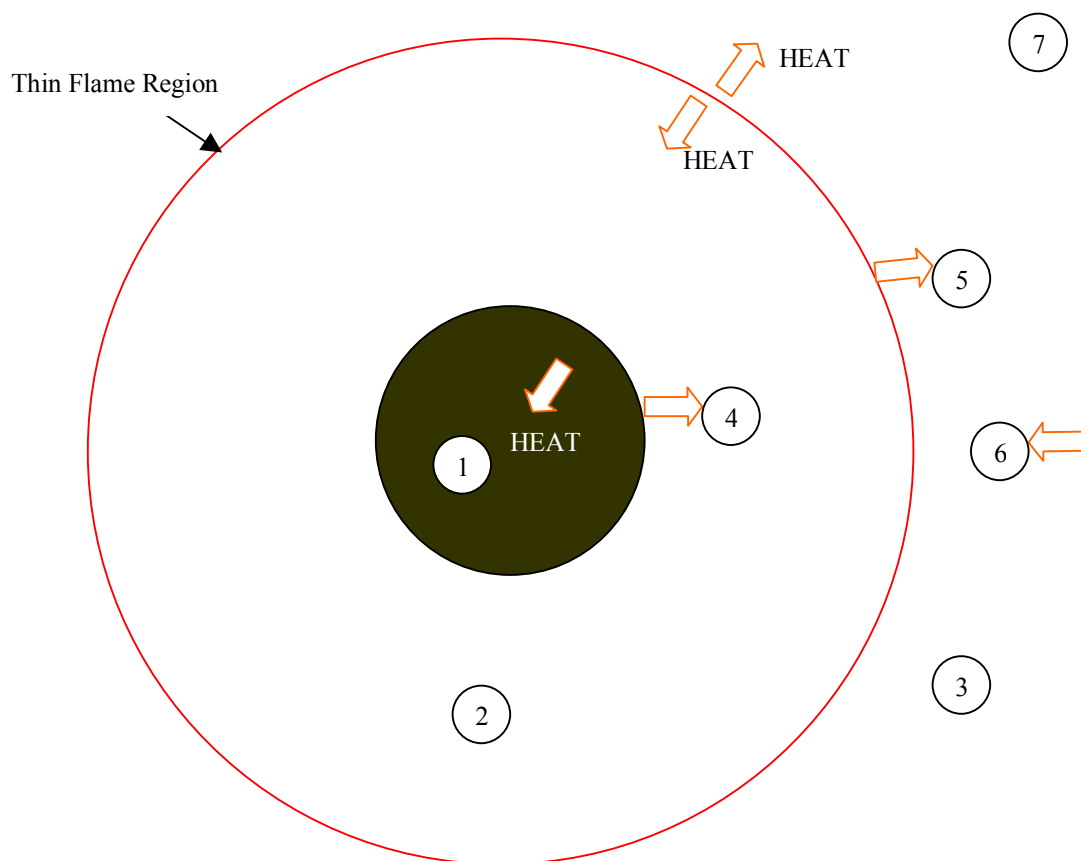


Fig. 2.1 Schematic of spherically symmetric droplet combustion.

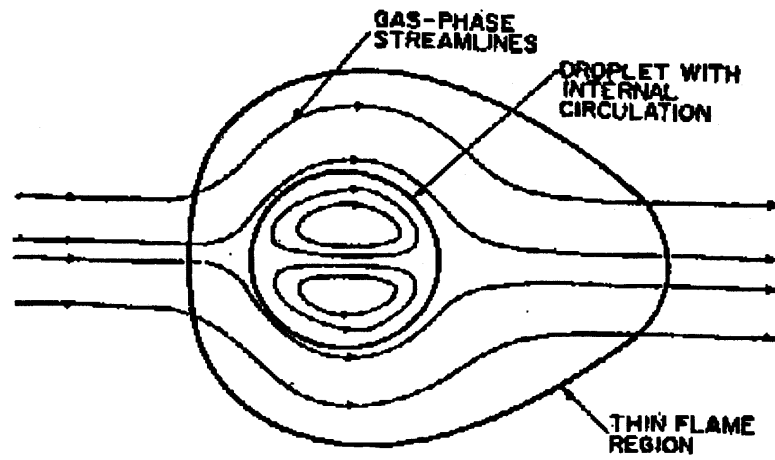


Fig. 2.2 Schematic showing convective droplet combustion without flow separation (Law<sup>7</sup>).

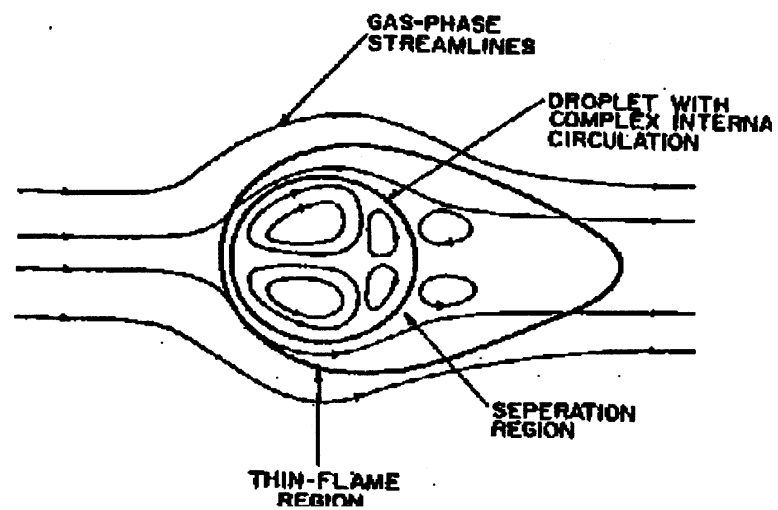


Fig. 2.3 Schematic showing convective droplet combustion with flow separation (Law<sup>7</sup>).

In the presence of either forced or/and natural convection, a non-radial relative velocity exists between the droplet and the surrounding gas. The shear stress exerted by the gas flow on the surface drags the liquid mass near the surface and hence induces a recirculatory motion within the droplet as shown in Fig. 2.2. For higher rates of external convection, flow separation occurs creating wake regions both inside and outside of the droplet as shown in Fig. 2.3. The presence of non-radial convection generally enhances the transport rates and thereby the gasification rate.

The theory behind  $d^2$ -law is that as gasification proceeds, the diameter of the droplet decreases with time. Most of the experimental data suggests linear correlation of  $d^2$  with time. The classical  $d^2$ -law for droplet combustion was formulated in the early 1950's by Godsave<sup>4</sup> and Spalding<sup>5</sup> assuming that gas phase chemical reaction is infinitely fast with respect to gas phase transport, thus confining chemical reaction to an infinitely thin sheet as shown in Fig. 2.4. The temperature and concentration profiles, which are typical of diffusion burning, is also illustrated. The other assumptions incorporated in the formulation of the  $d^2$ -law (Williams<sup>6</sup> and Law<sup>7</sup>) are stated in Table 2.1. The  $d^2$ -law theory predicts that the droplet burn rate, flame position, and flame temperature remain constant throughout the droplet burning lifetime.

In the  $d^2$ -law formulation, the droplet burn rate, flame standoff ratio and flame temperature are given by (Law<sup>8</sup>)

$$K = -\frac{d(d_s^2)}{dt} = \frac{8\rho D}{\rho_l} \ln(1+B) \quad (2.1)$$

$$\frac{r_f}{r_w} = \frac{\ln(1+B)}{\ln\left(1 + \frac{Y_{o,\infty}}{v_{o_2}}\right)} \quad (2.2)$$

**Classical d<sup>2</sup>-Law Model**  
 (Spalding, 1953; Godsave, 1953)

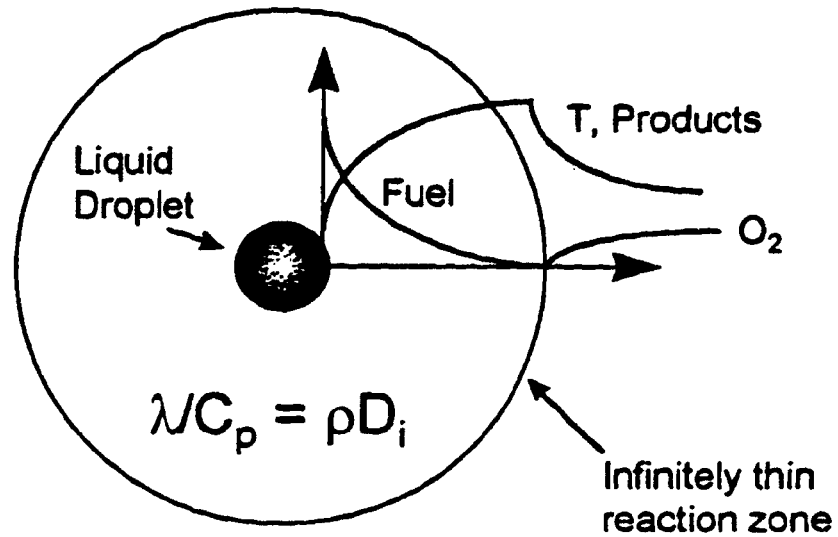


Fig. 2.4 Schematic of classical d<sup>2</sup>-law single droplet combustion model (Godsave<sup>4</sup>).

$$T_f = T_{ws} + \frac{T_\infty - T_{ws} + \frac{(h_c - L)Y_{o,\infty}}{c_{p,g}v_{o_2}}}{1 + \frac{Y_{o,\infty}}{v_{o_2}}} \quad (2.3)$$

Table 2.1. Assumptions incorporated in the formulation of  $d^2$ -law for droplet combustion

<ol style="list-style-type: none"> <li>1. Spherical symmetry</li> <li>2. Isolated droplet in infinite medium.</li> <li>3. Constant ambient pressure</li> <li>4. Chemical reaction infinitely fast compared to gas phase diffusion</li> <li>5. Quasi steady gas phase processes</li> <li>6. Uniform droplet temperature; no droplet heating</li> <li>7. Radiation effects from the droplet are neglected.</li> <li>8. Lewis number is assumed unity for all species in gas phase, i.e. <math>\rho D = \frac{\lambda}{c_p}</math></li> <li>9. Constant gas phase transport properties and thermal capacity.</li> <li>10. Negligible buoyancy.</li> </ol>
--

where  $r_w$  is the droplet radius,  $\rho_l$  the liquid density,  $\rho$  the gas density,  $r_f$  the flame radius,  $d_w$  is the droplet diameter,  $\alpha$  the evaporation ( $\alpha_{\text{evap}}$ ) or burning rate constant ( $\alpha_{\text{comb}}$ ),  $D$  the gas phase diffusion coefficient,  $B$  the Spalding transfer number,  $Y_{o,\infty}$  is the ambient oxygen mass fraction,  $\nu_{o_2}$  the stoichiometric oxidizer to fuel mass ratio,  $T_f$  the flame temperature,  $T_\infty$  the ambient temperature,  $T_w$  the droplet surface or wall temperature,  $h_c$  the heat of combustion of the liquid fuel and  $L$ , the latent heat of vaporization. The transfer number  $B$ , is a non-dimensional parameter measuring the ratio of drive toward vaporization through the heat of combustion (along with sensible enthalpy difference between the ambient environment and the droplet surface), divided by the resistance to vaporization through the heat of vaporization:

$$B = \frac{\frac{Y_{o,\infty} h_c}{\nu_{o_2}} + c_{p,g} (T_\infty - T_{ws})}{L} \quad (2.4)$$

For the combustion of most fuels in air, the Spalding transfer number is typically between 1 and 10.

Equations (2.1)-(2.3) reproduce experimental observations to varying degrees of accuracy. For single component droplets, the droplet burning rate is nearly constant over most of the droplet lifetime. Also, the qualitative predictions are quite correct as experiments show that the

burning rate increases with increasing  $\frac{\lambda_g}{c_{p,g}} \sim \rho D$  and decreases with increasing  $\rho_1$ . Quantitative

agreement between experiment and Equation (2.1) can also be achieved provided that appropriate selections of transport properties are made. The flame temperature predicted by Equation (2.3) is essentially the adiabatic flame temperature for the stoichiometric reaction between the liquid fuel and the oxidizer-inert mixture. Quantitative agreement in this case can be obtained by assuming suitable specific heat to account for dissociated products. The flame stand-off ratio, which under some experimental conditions can approach a constant value, is over-predicted by Equation (2.2). That the quantitative agreement is much worse for the flame position than for the burning rate is easily explained. The assumptions incorporated into the  $d^2$ -law analysis yield a flame position which is virtually independent of thermal/transport parameters. Thus, there are no parameters to choose to obtain quantitative flame temperature agreement. Thus, in summary, while the  $d^2$ -law (without use of suitable property  $\rho D$ ) has been pretty useful in a qualitative sense, it cannot simultaneously predict the burning rate, flame position and flame temperature. Fig. 2.5 shows the typical  $d^2$ -law burn rates, regression and flame front as a function of time.



Further experimental evidence (Kumagai *et al.*<sup>9</sup>, Law *et al.*<sup>10</sup>) on spherically symmetric droplet combustion over the years revealed certain qualitatively different behaviors, indicating the existence of serious weaknesses in the  $d^2$ -law. Fig. 2.6 shows that immediately after ignition, there exists a short period during which the droplet size changes very little (i.e. the burning rate is initially much lower than would be predicted by  $d^2$ -law). This is probably due to unsteady behavior in the initial periods.

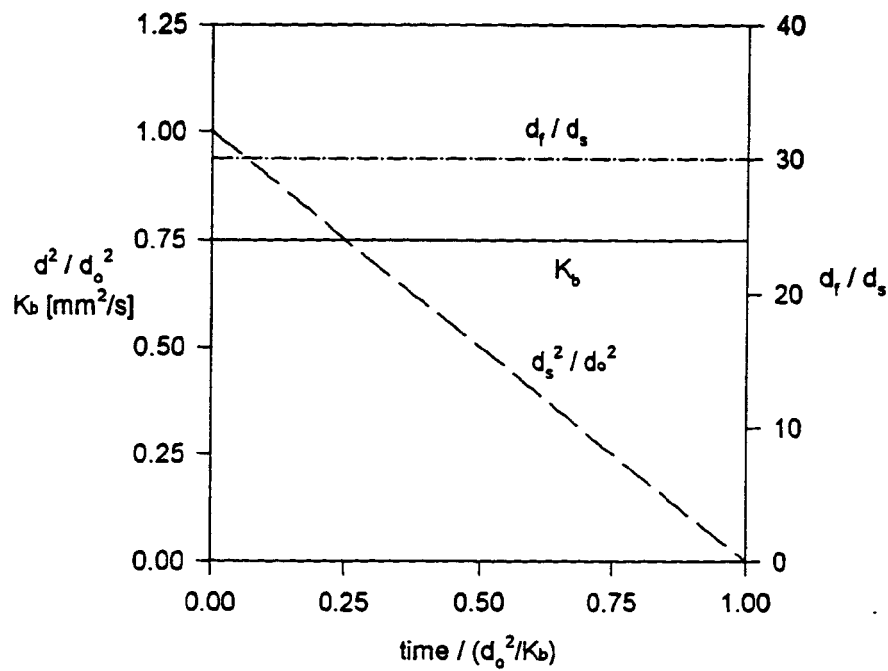


Fig. 2.5 Droplet surface regression, flame standoff ratio and burn rate as a function of time as predicted by quasi-steady formulation.

Secondly, the flame standoff ratio rather varies with time. For environments with low oxygen concentration, the flame standoff continuously increases while, for environments with higher oxygen concentration, the flame standoff initially increases and then approaches a constant value.

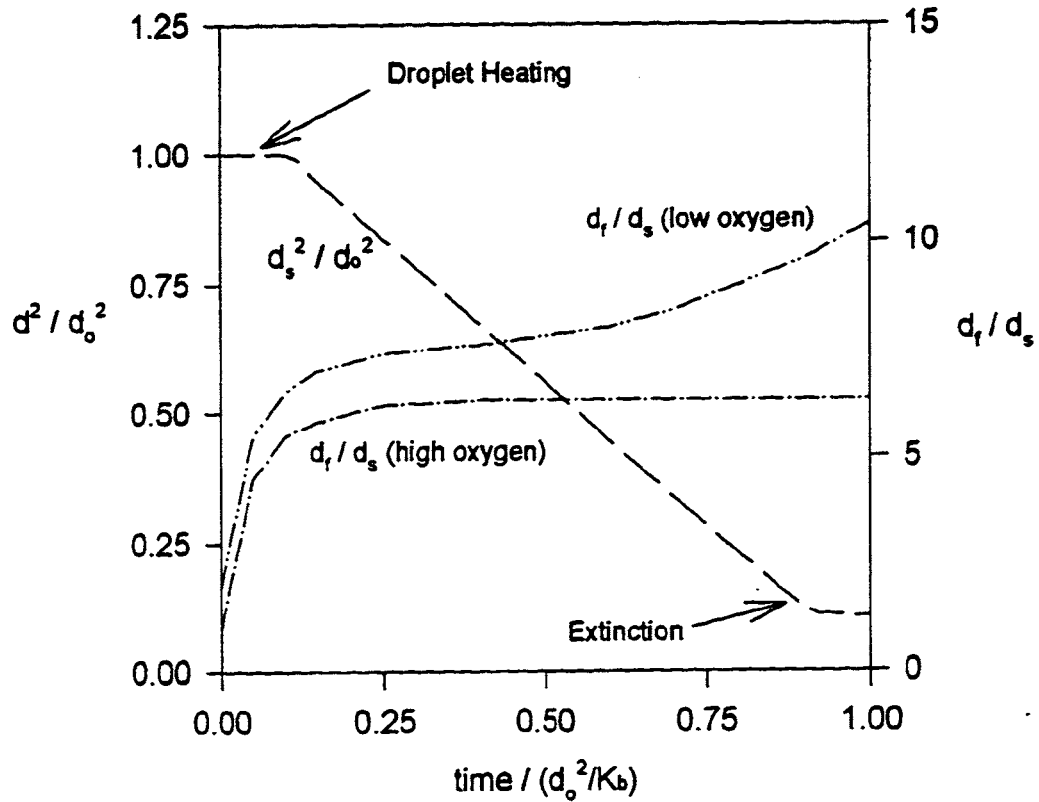


Fig. 2.6 Actual observations indicating heat up time and flame stand off variations as a function of time.

Both these deviations were found to be consequences of initial conditions which were not included in the  $d^2$ -law. By relaxing some assumptions the deviations were satisfactorily explained. The initial slow rate of surface regression is primarily due to the need to heat up the initially cold droplet to a temperature hot enough to sustain steady state burning; frequently this temperature is close to the liquid's boiling point under the prevailing pressure. An energy balance as shown in Fig. 2.7 at the droplet surface shows that heat conducted to the surface from the gas phase balances with the heat lost by conduction into the droplet interior and heat lost from the surface due to vaporization phase change. Initially, when the droplet temperature is

low, much of the heat is conducted inward, resulting in a lower rate of vaporization. Once the droplet heats up toward the liquid boiling point, little heat is conducted inward and the vaporization rate reaches its quasi-steady value. Since droplet heating and gasification are mutually exclusive, droplet heating is mostly over in about the first 10% of the droplet life time. For the remaining period,  $d^2$  should vary linearly with time. During multicomponent combustion, the droplet heating time differs depending upon components through their boiling points, latent heats and thermal properties.

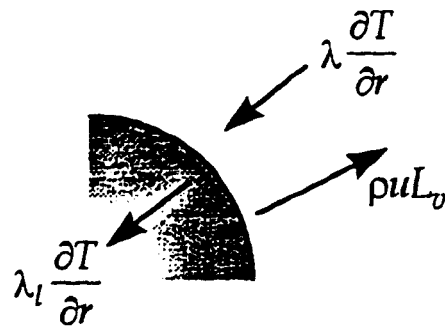


Fig. 2.7 Relaxation in  $d^2$ -law assumption: Energy equation at interface accounting for droplet heat-up.

Accounting for the accumulation of fuel vapor between the liquid droplet and the flame (Law<sup>8</sup>) explains the variation in flame position with time. In the  $d^2$ -law formulation, it is implicitly assumed that the rate of vaporization at the droplet surface is directly equal to the rate of consumption of fuel at the flame sheet. Initially, before ignition, the amount of fuel vapor present in the inner region as shown in Fig. 2.8 (between the droplet and flame) is less as the droplet temperature is low and steady state burning has not yet been achieved. At this stage, flame must lie closer to the droplet surface since fuel vapor mass fraction at the wall is low and

hence the stoichiometric surface is closer to the drop surface. As the droplet temperature increases to a steady state, the gasification rate is enhanced and the amount of fuel vapor accumulating in the inner region also increases. This causes the flame to move away from the surface. In environments with low oxygen concentration, the flame location continuously increases while in environments with higher oxygen concentration, the flame location reaches a steady state after some time (Law *et al.*<sup>10</sup>).

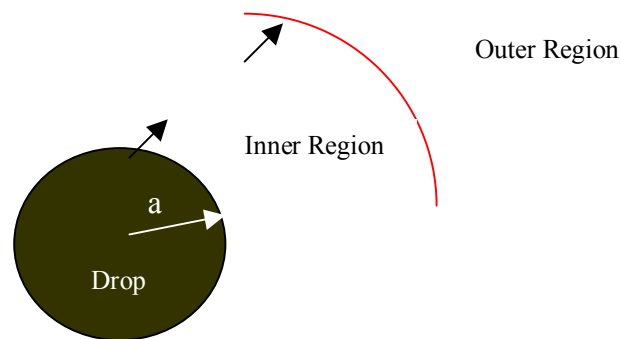


Fig. 2.8 Relaxation in  $d^2$ -law assumption: Vapor accumulation between flame and droplet.

Thus, by incorporating the following two corrections, a more accurate model can be developed. The droplet heating may be modeled by simply including a term for heat conduction to the droplet interior with the latent heat accounting for droplet vaporization. The amount of heat conducted inside can be determined by solving the temperature distribution within the droplet. The fuel accumulation can be accommodated by modifying the mass conservation equation to the following: *Gasification rate at droplet surface = Consumption rate at flame + Accumulation rate/Depletion rate in the inner region*. Figs. 2.7 and 2.8 show these two additions.

## 2.2 MULTICOMPONENT DROPLET COMBUSTION THEORY

The droplet combustion theory previously described used pure fuels. Recent trends in the design of engines and formulation of fuel blends indicate that multicomponent effects will become more prominent in the utilization of liquid fuels which are primarily used in the field of transportation. With more demand in improving fuel efficiency by controlling the process of combustion, the motivation to understand the multicomponent effects on combustion has increased. The widely different physical and chemical properties of the constituents of these hybrid fuels necessitate the study of multicomponent effects. In the study to such an effect, the relative volatilities of the constituents and their composition within the droplet demand consideration. The other factor to be considered would be the mixing of the constituents inside the droplet. This more or less influences the rate with which the liquid components can be brought to the surface where gasification occurs.

The gasification of the volatile component requires that it be brought to the surface before it can be gasified. The regressing droplet can be a way or it can be achieved passively through diffusion and internal mixing or circulation. The liquid phase mass diffusion is a very slow process and Landis and Mills<sup>11</sup> have shown that if it controls the rate, then there is a very high probability that the volatile and non-volatile components will be trapped within the droplet during most of the droplet lifetime. Under this situation the relative volatilities of the individual components cannot be the dominating factors in effecting gasification. On the other hand, in the presence of internal circulation Law<sup>12</sup> has shown that liquid-phase mass transport is facilitated such that the relative volatilities exert much stronger influence on the individual gasification rates. Thus, the combustion characteristics of a multicomponent droplet can be discussed in the two extreme rates of internal mixing, namely diffusion limit and distillation limit. In the former, there is no motion within the droplet interior such that diffusion is the only active transport

mode. In the latter, it is assumed that mixing occurs so fast that the states within the droplet interior are uniform.

In the formulation of a model for multicomponent combustion using a instantaneous mass transport (mixing) model, the overall burn rate, flame stand-off ratio and flame temperature are given by (Law<sup>12</sup>)

$$m_F = \ln(1 + B) \quad (2.5)$$

$$\epsilon_i = Y_{i,w} + (Y_{i,w} - Y_{i,f})(1 - Y_{F,w}) / (Y_{F,w} - Y_{F,f}) \quad (2.6)$$

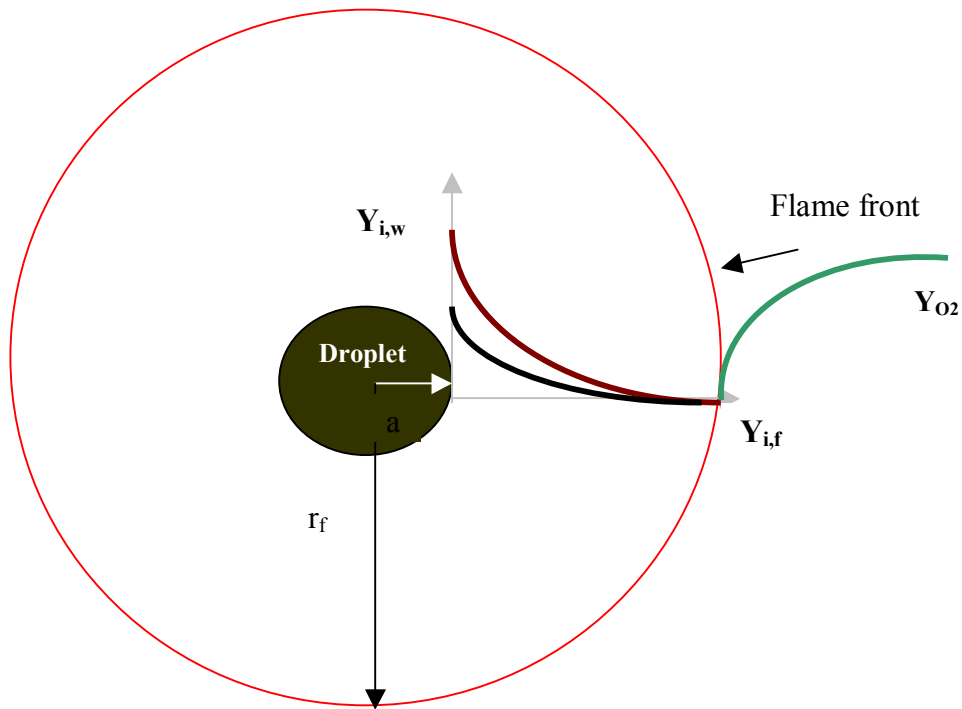


Fig. 2.9 Profile of multicomponent fuel vapor species in gas phase assuming flame sheet combustion.

$$r_f = \frac{[\ln(1+B)]}{\left[ \ln(1+\hat{Y}_{o,\infty}) \right]} \quad (2.7)$$

$$T_f = \frac{\left[ T_\infty - \hat{Y}_{o,\infty} \left( \hat{L} + \hat{H} - \hat{h}_c - T_w \right) \right]}{\left( 1 + \hat{Y}_{o,\infty} \right)} \quad (2.8)$$

where  $H$  is the heat input function and the species weighted quantities, designated by “ $\hat{\phantom{x}}$ ” are

$$\hat{L} = \sum \varepsilon_i L_i, \quad \hat{h}_c = \sum \varepsilon_i h_{c,i}, \quad \hat{\nu}_{o_2} = \sum \varepsilon_i \nu_{o_2,i}, \quad \hat{Y}_{o,\infty} = \frac{Y_{o,\infty}}{\hat{\nu}_{o_2}}, \quad \hat{m} = m/(4\pi\rho_g D_g r_w), \quad \varepsilon_i = m_i/m. \quad T \text{ is the}$$

non-dimensional temperature defined as  $C_p T'$  where  $T'$  is the temperature. The heat input

function and the transfer number  $B$  is given as

$$H = \frac{\left( T_\infty - T_w + \hat{L} - \hat{h}_c \right) + \left( 1 + \hat{Y}_{o,\infty} \right) \left[ \hat{h}_c - \hat{L} (1 - Y_{F,f}) / (1 - Y_{F,w}) \right]}{\left( 1 + \hat{Y}_{o,\infty} \right) (1 - Y_{F,f}) / (1 - Y_{F,w}) - 1} \quad (2.9)$$

$$B = \frac{\left( T_\infty - T_w + \hat{Y}_{o,\infty} \hat{h}_c \right)}{\hat{L} + \hat{H}} \quad (2.10)$$

The generalized expressions above can be solved for pure combustion by setting  $Y_{i,f} = Y_{F,f} = 0$  or for pure evaporation by setting  $Y_{o,\infty} = 0$  and  $Y_{i,f} = Y_{i,\infty}$ . Fig. 2.9 reveals qualitatively the profiles of a multicomponent fuel vapor species in gas phase for the formulation given above. If the states of the liquid remained quasi-steady during evaporation, as would be the case when all modes of heat and mass transport inside the droplet ceases, steady state evaporation prevails and

$H=0$  and the mass fractions in liquid phase of all the components remain constant. In reality, however, the droplet temperature and the composition vary temporally.

### 2.3 THESIS ORGANIZATION

This thesis presents a new formulation for multicomponent droplet combustion using double Shvab-Zeldovich coupling. An approximate approach is outlined and derived for a simple case of two component fuels, which can be extended to multiple components. The formulated model is applied to representative transportation fuels and validated with existing experimental data.

In Section 3, the objective of the thesis is outlined. The motivating factors behind the undertaking of the thesis are briefly stated.

In Section 4, the evaporation model and the newly formulated double Shvab-Zeldovich combustion model is discussed. The different assumptions which are incorporated in the formulation are outlined and the validity of the assumptions is explored. The formulation is based on the assumption of  $h_{c,o_2}$  values for different hydrocarbons. The results that have been outlined are for a two component fuel species and can be extended comfortably to multicomponent species.

In Section 5, the models described in Section 4 are validated with existing experimental data and the results presented and discussed. Since evaporation and combustion characteristics of transportation fuels of the likes of gasoline and diesel have not been explored so far, the model is used to get the approximate characteristics for some representative fuels of the kind. The evaporation model is applied to a gasoline droplet with discrete composition of hydrocarbons and the evaporation rates of the components of the droplet are determined. The results seem to indicate gasification resembling batch distillation. The model is then applied to diesel fuels represented by bi-component alkanes. The variation in composition of the volatile component is then plotted temporally and compared with experimental values. The variations closely matched



the qualitative behavior of the experiments. The quantitative deviations were more towards the latter part of the droplet lifetime when the experiments seemed to suggest a dominant factor in the name of diffusional resistance with decreasing volatility differentials among the components. The combustion model is then validated for a simple alcohol-alkane binary droplet. The burn-rate constant from experiment and the model matches closely. The model is then applied to representative diesel fuels and the results compared with experimental data. The numerical results matched appreciably with the experimental results. The results seem to suggest that the liquid phase diffusion limits burning to an extent.

In Section 6, results are summarized as to the formulation, application and validation and the limitations of the model are stated.

In Section 7, a brief overview of future work is presented. The current trends in multicomponent research are briefly mentioned.

The detailed derivation of the formulation is outlined in the Appendix.

### 3. OBJECTIVE

Over the years, for simplicity, fuels have been represented as a single component fuel in most multi dimensional models. However, single component fuel models have not been able to predict the complex behavior of the vaporization and combustion of multicomponent fuels of the likes of gasoline and diesel which are primarily used in the field of transportation. The preferential vaporization of light-end components in these multicomponent fuels greatly affects the fuel species distribution and ignition behavior near the spray and cannot be represented by single component fuel models.

The objective of the present work is divided into two categories:

1. To model the evaporation characteristics of multicomponent isolated transportation fuel droplets by applying the methodology developed by Annamalai *et al.*<sup>2</sup>. Evaporation characteristics of a discrete model of gasoline is of interest for analysis and is proposed to be predicted. The model will then be applied to representative diesel fuels and the results will be validated against existing experimental data.
- 2 To develop a model to evaluate the combustion characteristics of multicomponent isolated fuel droplets by using double Shvab-Zeldovich formulation. The model will then be validated against available experimental data for a multicomponent fuel and then applied to diesel fuels.

## 4. THEORETICAL FORMULATION OF EVAPORATION AND COMBUSTION MODELS

### 4.1 INTRODUCTION

In this section, the evaporation and combustion models applicable to evaluate the vaporization characteristics of multicomponent droplets are described. The evaporation model is used to predict the evaporation characteristics of discretely compositional droplet of gasoline and diesel fuels. The combustion model is based on double Shvab-Zeldovich coupling of the vapor species of the multicomponent fuel.

### 4.2 DROPLET EVAPORATION MODEL

A spherical liquid droplet with a large number of components vaporizing without chemical reactions, in a relatively low-pressure (ambient) gaseous environment is considered. The droplet evaporation calculations presented in this section were performed using the quasi steady, uniform- temperature-concentration model developed by Annamalai *et al.*<sup>2</sup> The numerical model simulates a spherically symmetric, isobaric evaporation of a multicomponent fuel droplet in an infinite stagnant ambience. The computations consider molecular transport and energy transport in the gas phase; liquid-vapor equilibrium at the droplet surface. The droplet temperature and compositional variation are then passively computed. In this section, the equations governing the gas-phase and vapor-liquid interface are described along with the boundary and initial conditions.

The situation considered is a spherically symmetric evaporation of a multicomponent droplet of radius  $a$ , temperature  $T_w$  and consisting of compounds characterized by their respective mass fractions  $Y_i$ , molecular weights  $W_i$ , latent heats of vaporization  $L_i$ , normal boiling temperatures at atmospheric pressure  $T_{bp}$ . The atmosphere is characterized by temperature  $T_\infty$ , pressure  $P_\infty$ , and

mass fractions  $Y_{o,\infty}$  of an oxidizing gas 'o' and  $Y_{I,\infty}$  of an inert gas, say nitrogen. For the case of evaporation we assume that there is no oxidizing environment present and set  $Y_{o,\infty}$  to zero.

#### 4.2.1 Gas Phase

With the utilization of the assumptions that the gas phase is quasi-steady and that the droplet has infinite thermal conductivity and diffusivity, the species and mass conservation equations can be solved to get the flux ratios  $\varepsilon_i$  and evaporation rate  $\zeta_i$  of an  $N$  component fuel. The conservation equations of mass, species and energy presented below are sufficient to describe the spherically symmetric gas phase surrounding the liquid droplet (Williams<sup>13</sup>):

$$\frac{1}{r^2} \frac{\partial}{\partial r} (r^2 \rho_g v_r) = 0 \quad (4.1)$$

$$\frac{d}{dr} (\rho_g v_r 4\pi r^2 Y_{g,i}) = \frac{d}{dr} \left( \rho_g D_g 4\pi r^2 \frac{dY_{g,i}}{dr} \right) \quad (4.2)$$

$$\frac{d}{dr} (\rho_g v_r 4\pi r^2 Y_{g,i}) = \frac{d}{dr} \left( \frac{\lambda_g}{c_{p,g}} 4\pi r^2 \frac{dh_T}{dr} \right) \quad (4.3)$$

where  $\rho_g$  is the density of the gas mixture,  $c_{p,g}$  the specific heat of the gas mixture at constant pressure,  $\lambda_g$  the thermal conductivity of the gas mixture,  $Y_{g,i}$  the mass fraction of the  $i^{\text{th}}$  species in the gas phase,  $T_g$  the temperature of the gas mixture,  $h_i$  the thermal enthalpy of the gas phase species,  $v_r$  the fluid velocity in the radial direction,  $r$  the radial coordinate. The density of the fuel vapor species in the gas phase is assumed to be governed by the ideal gas equation of state:

$$\rho_g = \frac{P_\infty}{RT_g} \left[ \sum_{i=1}^n \frac{MW_i}{Y_{g,i}} \right] \quad (4.4)$$

To get the species and the temperature profiles, Equations (4.2) and (4.3) are integrated over the spatial coordinate with appropriate boundary and initial conditions. For the calculations described in this thesis, temperature-average formulations are employed to evaluate the gas phase property of interest namely the binary diffusion coefficient. It is evaluated using the Chapman-Enskog formulation (Turns<sup>14</sup>) which utilizes the Lennard-Jones potential well depth and collision diameter. The value of  $\rho_g D_g$  is assumed to be constant for all vapor species. Thus, this product for a representative species is used for computations. The binary diffusion coefficient is computed using the following relationship:

$$D_{AB} = \frac{3}{16} \frac{(4\pi k_B T / W_{AB})^{1/2}}{(P_\infty / RT) \pi \sigma_{AB}^2 \Omega_D} \quad (4.5)$$

Usually, the overall properties of the mixture vary considerably throughout the gas phase. The variation in the overall mixture properties is due to the variation in temperature as well as species concentrations throughout the gas phase. Most of the earlier droplet combustion theories assume unity Lewis number for each gas phase species. The Lewis number of each  $i^{\text{th}}$  species is defined as:

$$Le_i = \frac{(\lambda / c_p)_g}{\rho_g D_i} \quad (4.6)$$

where  $D_i$  is the mass diffusivity of the  $i^{\text{th}}$  species as calculated by Equation (4.5). The evaporation model used in this thesis uses the unity Lewis number assumption, wherein  $\lambda/c_p$  is set equal to  $\rho D$ . The solution for the temperature and the compositional variation in the gas phase is given by: (Annamalai *et al.*<sup>2</sup>)

$$\frac{Y_i - Y_{i,\infty}}{Y_{i,w} - Y_{i,\infty}} = \frac{1 - e^{-\xi}}{1 - e^{-\xi_{w,iso}}}, i = 1 \dots N \quad (4.7)$$

$$\frac{h_T - h_{T,\infty}}{h_{T,w} - h_{T,\infty}} = \frac{1 - e^{-\xi}}{1 - e^{-\xi_{w,iso}}}, i = 1 \dots N \quad (4.8)$$

where the non-dimensional  $\xi$  is defined as (Annamalai<sup>15</sup>)

$$\xi = \frac{m_{iso}}{4\pi\rho Dr}; \xi_w = \frac{m_{iso}}{4\pi\rho Da} \quad (4.9)$$

Using interface species and energy equation, the fuel species mass fraction at the droplet surface is given as:

$$Y_{i,w} = \frac{h_{T,\infty} \varepsilon_i}{\sum L_i \varepsilon_i + h_{T,\infty}}; i = 1 \dots N \quad (4.10)$$

where  $\varepsilon_i$  is defined as

$$\varepsilon_i = \frac{m_i}{m} \quad (4.11)$$

We define the variable  $h_i$  as the thermal enthalpy given by:

$$h_T = c_p (T - T_w) \quad (4.12)$$

Setting the thermal enthalpy at the droplet wall as the reference value and utilizing the interface energy conservation, the evaporation rate is obtained as

$$\xi_w = \ln \left[ 1 + B_{evap} \right] \quad (4.13)$$

where  $B_{evap}$  is called as the transfer number for evaporation defined as

$$B_{evap} = \frac{h_{T,\infty}}{L_{multi}}, \quad L_{multi} = \sum L_i \varepsilon_i \quad (4.14)$$

One may verify that the result given by Equation (4.14) is identically same as the one given by Law in Equation (2.10) when one sets  $Y_{0,\infty}=0$  in Equation (2.10).

#### 4.2.2 Vapor-Liquid Interface

At the liquid-vapor interface, the vapor and liquid phases are assumed to be in equilibrium. For a liquid-vapor system in equilibrium, the gas phase mole fractions at the droplet surface,  $X_{g,i}$  are related to the liquid phase mole fractions,  $X_{l,i}$  through the following relation:

$$X_{g,i} = X_{l,i} \frac{p_i^{sat}}{P_\infty} \quad (4.15)$$

where  $p_i^{sat}$  is the saturation pressure of the pure  $i^{\text{th}}$  component, and  $P_\infty$  is the total pressure. It is to be noted that the gas phase is assumed to be a mixture of perfect gases as the solution is assumed to be ideal. This equation is representative of Raoult's law where the vapor is assumed to be saturated. Furthermore, the partial pressure of each component in the mixture is evaluated using the Clausius-Clapyron equation. Thus, the partial pressure of each pure  $i^{\text{th}}$  component is computed using the following relation:

$$p_i^{sat} = P^0 \exp\left(\frac{-L_i W_i}{R}\right) \left(\frac{1}{T_w} - \frac{1}{T_{bp,i}}\right) \quad (4.16)$$

where  $T_{bp,i}$  refers to the boiling temperature of the pure species  $i$  at  $P^0=1\text{bar}$ . In order to calculate the flux ratios of the individual components, Equation (3.10) is used. The molar and mass fractions are related through

$$Y_i = \frac{X_i W_i}{\sum X_i W_i} \quad (4.17)$$

Using Equations (4.9)-(4.14), the evaporation rate of the isolated fuel droplet and the individual species can be determined. The other parameters of interest including the changes occurring in the liquid phase are discussed in detail in the next section.

### 4.3 DROPLET COMBUSTION MODEL

The previous section outlined the gas phase heat and mass transfer controlled vaporization of a multicomponent droplet in a stagnant, unbounded atmosphere. The combustion model described in this section is a simple way of determining the combustion rate of a multicomponent fuel. The development of this model is warranted because most of the liquid fuels employed in engines and power plants are mixtures of many chemical compounds with widely different volatilities. For example, a typical gasoline fuel consists of over 200 hydrocarbons which range from a lower boiling point of 300K to a final boiling point that can be as high as 500K. It is henceforth uncertain that a single, representative surrogate fuel can be selected such that the single component droplet vaporization theory be utilized to predict the evaporation and combustion behavior of a multicomponent fuel. Although the extremes in the



characteristics can be estimated by representing the fuel by its least or most volatile component, such results will be far from the exact mechanism required for optimal design considerations.

The two complexities that are considered in comparison with a single droplet model are the following. Firstly, the species vapor transport in the gas phase and the phase change process at the interface are to be understood. Secondly, since in reality the evaporation process is time varying due to the continuous change in temperature and composition of the droplet as vaporization proceeds it is important to understand the heat and mass transport within the liquid.

The assumptions used in developing this model are explored in detail in this section and its validity explored. Then, the formulation of the model is explained from the basic conservation equations. The detailed derivation of the calculation of the parameters of interest is shown in Appendix A and B.

#### 4.3.1 Assumptions

The problem analyzed is a spherically symmetric vaporization of a multicomponent droplet of radius  $a$ , temperature  $T_w$  and consisting of compounds characterized by their respective mass fractions  $Y_{i,l}$ , molecular weights  $W_i$ , latent heats of vaporization  $L_i$ , normal boiling temperatures at atmospheric pressure  $T_{bp}$ . The atmosphere is characterized by temperature  $T_\infty$ , pressure  $P_\infty$ , and mass fractions  $Y_{o,\infty}$  of an oxidizing gas 'o' and  $Y_{I,\infty}$  of an inert gas, say nitrogen. During combustion, it is assumed that the outwardly diffusing multicomponent fuel vapor  $F$  reacts stoichiometrically and completely with the inwardly diffusing oxidizer gas at an infinitely thin flame-front located at  $r_f$  where  $\sum Y_{i,r} = 0$  for the  $N$  vaporizing species.

It is further assumed for simplicity that the gas phase thermal conductivity coefficients  $\lambda_g$  and specific heats  $c_g$  of the various species are constants and equal to each other, and that the gas phase Lewis number  $Le = \lambda_g / (c_p \rho D)$  is unity. The formulation can be extended for variable properties at the expense of complicated mathematics.

The other parameters to be accounted for are the gas phase heat and mass transfer rates, liquid phase heat and mass transfer rates and the rate at which the droplet surface regresses. Due to higher liquid to gas density ratio, the liquid phase has higher mass and thermal inertia compared to gas phase. Hence, the states at the droplet surface can be considered almost frozen compared to the characteristic gas phase transport time. Thus it is justified to assume that the gas phase processes are quasi steady.

It is also assumed in the formulation that internal circulation (mixing) is the rate-controlling process rather than liquid phase diffusion. Hence, it is assumed that the temperature and species concentrations within the droplet are maintained uniform (infinite thermal conductivity and mass diffusivity) due to circulation due to high diffusivity though this need not be the case always. As an additional note, it is to be understood that internal circulation can either be produced during the initial violent atomization process or arise as a result of natural or forced convection due to different densities of various components, which induces shear stress at the droplet surface. In either case, it is assumed that the droplet ceases to be viscous.

#### 4.3.2 Gas Phase

With the above assumptions, the gas phase continuity, species and energy equations can be written in vectorial form as:

$$\nabla \cdot (\rho \vec{v}) = 0 \quad (4.18)$$

$$\nabla \cdot (\rho \vec{v} Y_i - \rho D \nabla Y_i) = \dot{w}_i^m ; i=1 \dots N \quad (4.19)$$

$$\nabla \cdot (\rho \vec{v} h_T - \rho D \nabla h_T) = \dot{q} \quad (4.20)$$

where  $\dot{w}_i$  is the rate at which species  $i$  is consumed or produced, and  $\dot{q}$  is the rate at which heat is generated chemically. For each of the species and energy equations, the first and second terms on the left hand side represent the convective and diffusive transport, while the right hand side is the chemical source/sink term. Since transportation fuels of the likes of gasoline, diesel, and kerosene are made of complex mixture of hydrocarbons whose detailed oxidation kinetic mechanism is not known, the detailed kinetics is approximated as a one step overall reaction between the fuel  $F$  and the oxidizer  $o$ .



where  $\nu_{o_2,i}$  is the stoichiometric mass coefficient of the oxidizer per unit mass of fuel species  $i$  consumed and  $h_{c,i}$  is the associated heat release with species  $i$ . The fundamental equations in the case of multicomponent combustion problem are highly non-linear and coupling with the  $Y_i$  and  $T$  variations offer a mathematical challenge. The combustion rate is determined by the formulation described below which uses double Shvab-Zeldovich coupling.

A linear coupling of the species and energy equations described in Appendix A eliminates the reaction term and the following coupled equation is obtained:

$$\nabla \cdot (\rho \vec{v} \beta - \rho D \nabla \beta) = 0 \quad (4.22)$$

The variable  $\beta$  is called as the Shvab-Zeldovich variable, which is defined in any of the following ways depending on the nature of coupling. For a multicomponent fuel comprising of  $i$  species defined by the fundamental Equations (4.19) and (4.20), the Shvab-Zeldovich variable

coupling the fuel and oxidizer species is given as: (the variable is defined for just two species A and B here. It can be similarly extended to i species.)

$$\beta_{O_2-A-B} = Y_{o_2} - \nu_{O_2,A} Y_A - \nu_{O_2,B} Y_B \quad (4.23)$$

The variable can also be defined by coupling the fuel species with the energy equation. Such a coupling yields the Shvab-Zeldovich variable as:

$$\beta_{h_T-A-B} = h_T + Y_A h_{c,A} + Y_B h_{c,B} \quad (4.24)$$

By defining the Shvab-Zeldovich variable in any of the following ways through a coupling function, we get a chemically inert differential equation which is solved for  $Y_i$  and is then substituted back in the energy equation to get the temperature distribution. This solution involves a devious procedure of non-dimensionalizing the parameters and solving.

A novel way is developed in this thesis to simplify the computation of combustion parameters of interest without losing the exactness of the physics behind the problem. The approach makes use of the coupling between the oxidizer species and the energy equation to obtain a modified Shvab-Zeldovich variable. A new variable  $h_{c,o_2}$  is defined in the process. This variable represents the heating value of fuel per unit mass of stoichiometric oxygen consumed. It was found that this value was similar for all hydrocarbons found in fuels of the likes of gasoline and diesel. Table 4.1 summarizes this value for some hydrocarbons found in gasoline and diesel. Such a coupling gives the modified Shvab-Zeldovich variable as:

$$\beta_{h_T-o_2} = Y_{o_2} + \frac{h_T}{h_{c,o_2}} \quad (4.25)$$

Table 4.1. Values of  $h_{c,o_2}$  for some representative hydrocarbons found in gasoline and diesel

Component	$h_c$ (kJ/kg)	$h_{c,o_2}$ (kJ/kg)
n-butane	49138	13726
n-pentane	48635	13700
n-hexane	48309	13684
n-heptane	48073	13696
n-octane	47886	13682
benzene	41837	13630
toluene	42436	13558
decane	47638	13638
dodecane	47477	13635
tetradecane	47440	13671
hexadecane	47249	13617

To obtain the burn rate of the isolated fuel droplet, this variable is solved for using Equation (4.22). The non-dimensional burn rate is then obtained as:

$$\xi_w = \ln(1 + B_{comb}) \quad (4.26)$$

where  $B_{comb}$  of a multicomponent droplet is defined as the transfer number for combustion.

$$B_{comb} = \frac{Y_{o_2,\infty} + \frac{h_{T,\infty}}{h_{c,o_2}}}{\frac{L_{multi}}{h_{c,o_2}}} \quad (4.27)$$

This relationship for the transfer number is a very simple expression involving the latent heat for the multiple species. In this case,  $L_{multi}$  is given by:

$$L_{multi} = L_A \epsilon_A + L_B \epsilon_B \quad (4.28)$$

The flux ratios or the fractional rate of combustion are required for the individual species in order to get the burn rate of the fuel droplet. By invoking the previously stated assumption that the reaction proceeds with an infinitely fast rate at an infinitesimally thin flame location  $r_f$  and that the flame location for component  $A$  is same as that for component  $B$ , a simple relationship is obtained for the flux ratios. It is also the location where fuel species mass fractions are in stoichiometric proportion to the oxidizer mass fraction, i.e.  $Y_A \nu_{o2,A} + Y_B \nu_{o2,B} = Y_{o2}$ . The solution of the species equations using the above assumption (Appendix C) yields:

$$\frac{1}{(1 - Y_{I,w})} = \frac{\epsilon_i}{Y_{i,w}} \quad (4.29)$$

$$\text{Note that } 1 - Y_{i,w} = Y_{F,w} = \sum Y_{i,w}$$

### 4.3.3 Interface boundary conditions

The approximate burn rate is obtained by applying the energy and interface boundary conditions and coupling them as shown below. The interface energy and species conservation are given as:

$$\left( \frac{\partial h_T}{\partial \xi} \right)_w = -(L_A \epsilon_A + L_B \epsilon_B) \quad (4.30)$$

$$\left( \frac{\partial Y_i}{\partial \xi} \right)_w + Y_{i,w} = \epsilon_i \quad (4.31)$$

To obtain the burn rate, the boundary conditions are coupled to get a resultant condition given by:

$$\left( \frac{\partial \beta_{h_T}}{\partial \xi} \right)_w + \beta_w = -L_{multi} + h_{c,multi} \quad (4.32)$$

where  $L_{\text{multi}}$  has already been defined. Applying this boundary condition and solving for the burn rate yields the transfer number in terms of  $F$  and  $O_2$  as:

$$B_{\text{comb}} = \frac{\left( -Y_{F,w} - \frac{Y_{O_2,\infty}}{v_{O_2,\text{avg}}} \right)}{(Y_{F,w} - 1)} \quad (4.33)$$

The final solution for the burn rate needs the computation of the droplet surface temperature. The new method described above is used to obtain the droplet temperature by comparing the values of the fuel vapor mass fraction and iterating. A new variable 's' is defined to obtain the fuel mass fraction. The equation relating the two is given as:

$$Y_{F,w} = 1 - \frac{(1 + s)}{(1 + B_{\text{comb}})} \quad (4.34)$$

A brief understanding of the phase change relations is required to obtain the desired parameter.

#### 4.3.4 Phase Change Relations

Since the phase change processes usually occur at rates much faster than the gas phase transport rates, it is expected that the fuel vapor is always saturated at the droplet surface during evaporation. The partial saturation vapor pressure  $p_{i,w}$  of each component at the droplet surface can be determined by assuming that the liquid mixture behaves as an ideal mixture such that Raoult's law is satisfied. Hence:

$$p_{i,w} = X_{i,l} P_{i,l}^{\text{sat}} \quad (4.35)$$

This equation states that the partial pressure for species  $i$  in a mixture is proportional to its vapor pressure when it is in the pure state, the proportionality constant being its mole fraction in the mixture. This assumption that the mixture behaves ideally is the simplest conceivable, from either a mathematical or physical viewpoint. The equilibrium vapor pressure for the pure liquid is then given by Clausius-Clapyron relation already discussed in Equation (4.16). The mass fractions of the different components are then evaluated using Equation (4.17).

#### 4.3.5 Solutions

Now that the mass fractions of the fuel species have been obtained for assumed  $T_w$ , the flux ratios are evaluated using Equation (4.28). The transfer number is then estimated using Equation (4.27) and it is used to calculate the new fuel mass fraction using Equation (4.33). This value is then compared with the value for mass fraction obtained using Raoult's law. The wall temperature is then iterated till the two values for the mass fractions match. It is then possible to get an explicit relation for flame location using the solution for the species equation involving the modified SZ variable  $\beta_{o_2-F}$  and invoking the thin flame assumption. Since we are not interested in the location of the flame, the derivation is confined to Appendix D.

If the liquid properties are assumed to remain uniform, then all modes of transport within the droplet are suppressed. At this stage,  $X_{i,l}$  is constant and steady-state vaporization prevails. Knowing  $T_w$ , all other parameters of interest can be evaluated. The steady-state vaporization problem is completely solved at this stage.

In reality, the droplet temperature  $T_w$  and concentration  $X_{i,l}$  continuously change. Since the drop temperature keeps increasing as the drop evaporates, the latent heat must be modified to include sensible heat,  $L_{\text{sensible}} = L + c_p(T_w(t) - T_{\text{initial}})$  where  $T_{\text{initial}}$  is the temperature during initial period of drop vaporization. The next section will discuss these and the variations in diameter.



### 4.3.6 Liquid Phase Balance

After time  $t$ , the droplet mass shrinks by an amount given by:

$$m_{iso} = m_{iso,t_0} - \dot{m}_{iso} \Delta t \quad (4.36)$$

$$m_{iso,i} = m_{iso,i,t_0} - \dot{m}_{iso,i} \Delta t \quad (4.37)$$

where  $\Delta t = t - t_0$  and  $m_{iso,i}$  is the mass fraction of component  $i$  remaining in the droplet at  $t = t_0 + \Delta t$ .

Also

$$m_{iso} = \sum_i m_{iso,i} \quad i=A,B,\dots \quad (4.38)$$

and

$$Y_{i,t} = \frac{m_{iso,i}}{m_{iso}} \quad (4.39)$$

Since  $m_{iso} = \frac{\pi}{6} d_w^3 \rho_{mix}$  where  $d_w$  is the regressing droplet diameter and  $\rho_{mix}$  is the density of the

mixture varying temporally defined by:

$$\rho_{mix} = \sum_l \rho_{i,l} Y_{i,l} \quad (4.40)$$

Droplet regression can be written as:

$$d_w^3 = \frac{6m_{iso}}{\pi\rho_{mix}} \quad (4.41)$$

where the varying mass of the droplet and density of the mixture has been defined previously. Knowing instantaneous  $Y_{1,i}$ , we can get mole fraction of  $i$ . Alternately, one can obtain individual mole fractions using

$$X_{i,t} = \frac{N_{i,t}}{\sum N_{i,t}} \quad (4.42)$$

where the varying number of moles of individual species  $i$  in liquid phase is given by:

$$N_{i,t} = N_{i,0} - \frac{m_i dt}{MW_i} \quad (4.43)$$

The variation of composition with time is evaluated iteratively in a loop for various time intervals until diameter is reduced to zero. At every time interval the droplet temperature can be found iteratively with the knowledge of individual species mass fractions.

## 5. RESULTS AND DISCUSSION

### 5.1 INTRODUCTION

The present evaporation and combustion model was applied to study the vaporization and combustion of a single, stagnant multicomponent droplet. The results to be presented for pure vaporization include the case of a discrete compositional gasoline droplet followed by the application of the model to a combination of representative diesel fuels. Results are presented for droplet diameter for gasoline and evaporation rates of the individual species evaluated. For the diesel fuels, the model was applied to evaluate the concentration profiles of the volatile component, trace their temporal profile and to compare them with experimental results.

To investigate the salient features of the combustion model, a two-component mixture consisting of an alcohol-alkane namely octanol and undecane was selected for study. The combustion model was applied to the mixture and the results are validated with the experimental values of Law and Law<sup>16</sup>. Later, the combustion model was applied to investigate the temporal concentration profiles of representative diesel fuels already investigated for vaporization and the results compared with the experimental data of Randolph et al<sup>17</sup>.

### 5.2 EVAPORATION RESULTS

#### 5.2.1 Gasoline Droplet

Gasoline droplet was modeled as a discrete compositional multicomponent droplet rather than a continuous composition model, thereby avoiding the continuous thermodynamics method which represents the fuel composition as a continuous distribution function with respect to an appropriate parameter such as molecular weight. The discrete compositional model facilitates the solving of transport equations for each species in order to track the fuel composition and vaporization behavior.

The physico-chemical and thermodynamic properties (Gallant<sup>18,19,20</sup>, Chemnetbase<sup>21</sup>) are summarized in Table 5.1. Initially, the environment is assumed to be devoid of any fuel vapor. For calculation purposes, the gas phase specific heat was taken to be that of the fuel vapor at an average temperature of  $(T_{\infty}+T_w)/2$ . Using the expression from Borman and Ragland<sup>22</sup>, it was calculated as 1.942 kJ/kg-K.

Table 5.1. Thermodynamic properties and composition of the components of gasoline (Hamilton<sup>23</sup>)

Component	$\rho_{25^{\circ}C}$ (kg/m <sup>3</sup> )	W(kg/kmol)	L <sub>bp</sub> (kJ/kg)	T <sub>bp</sub> (K)	X <sub>i</sub>
<b>Normal paraffins</b>					
n-butane	573	58.12	386.08	272.65	0.03
n-pentane	626	72.15	357.45	309.21	0.03
n-hexane	661	86.18	334.78	341.88	0.03
n-heptane	680	100.2	317.05	371.55	0.03
n-octane	699	114.23	301.23	398.82	0.03
<b>Cycloparaffins</b>					
Cyclopentane	746	70.13	393.55	322.45	0.06
Cyclohexane	774	84.16	355.88	353.95	0.06
<b>Aromatics</b>					
Benzene	877	78.11	393.28	353.24	0.175
Toluene	867	92.14	360.1	383.78	0.175
<b>Olefin</b>					
Cyclopentene	772	68.11	376.81	317.35	0.08
<b>Isoparaffins</b>					
2 methyl propane	551	58.12	360.06	261.45	0.15
2 methyl butane	620	72.15	339.13	300.95	0.15

The ambient temperature and pressure were taken as 1000K and 1 bar respectively. The flux ratio and rate of evaporation of each component of gasoline was evaluated using the approach outlined in the previous section. Table 5.2 summarizes the input parameters used for evaporation calculations.

Table 5.2. Input data for isolated gasoline droplet evaporation

Fuel Diameter = 600microns
<b>Ambient conditions</b>
Temperature ( $T_{\infty}$ ) = 1000K
Pressure ( $P_{\infty}$ ) = 1 bar
<b>Transport properties</b>
$c_p = 1.942$ kJ/kg-K
$\rho D = 2.047 \cdot 10^{-5}$ kg/m-sec

The atmosphere is air and the only pressure considered was 1 atm (1 bar) because, apart from the slight pressure dependence of the various thermo-physical properties, its only influence on the model is through evaluation of the surface mole fractions, with obvious implications. All the ambient fuel vapor concentrations were set to zero for simplicity, hence excluding the possibility of condensation of any species. The results of the evaporation rates and flux ratios are summarized in Table 5.3.

Table 5.3. Evaporation rates of the components of representative gasoline fuel vaporizing at  $T_{\infty}=1000\text{K}$ ,  $P_{\infty}=1\text{bar}$  with  $c_p=1.942\text{kJ/kgK}$  and  $T_w=284\text{K}$

Component	$\dot{m}_i \times 10^{-9} \text{ (kg / sec)}$	$\epsilon_i$
2 methyl propane	70.37	0.5785
2 methyl butane	19.00	0.1562
n-butane	9.53	0.0783
cyclo pentene	7.28	0.0599
benzene	4.46	0.0367
cyclo pentane	4.13	0.0339
n-pentane	2.79	0.0229
toluene	1.43	0.0117
cyclo hexane	1.37	0.0113
n-hexane	0.89	0.0073
n-heptane	0.30	0.0025
n-octane	0.11	0.0009

The calculated diameter ( $d^2$  as a function of time) for a gasoline droplet, is shown in Fig. 5.1. Droplet surface area decreases gradually with time from the beginning and the evaporation constant, which is defined as the negative of the gradient of the surface regression curve, i.e.,  $\alpha_e = -(dD^2/dt)$  was obtained as  $0.344 \text{ mm}^2/\text{sec}$ . Fig. 5.2 portrays the relative volatilities of the components of the gasoline droplet considered. The relative volatilities is measured as a ratio of the mole fraction of the components in the gaseous phase to that in the liquid phase at different temperatures. It can be easily observed that 2-methyl propane is the most volatile component and n-octane, the least volatile at all temperatures considered. For all calculations, the initial droplet diameter was taken as  $600\mu\text{m}$  and  $\rho D$  ( $=\lambda/c_p$ ) was assumed constant and evaluated as  $2.047 \times 10^{-5} \text{ kg/m-sec}$ . It is important to infer that gasoline droplets do not reach a steady temperature, as in the case of single component droplets. This is because the composition of the droplet is continuously changing as the more volatile components are vaporized.

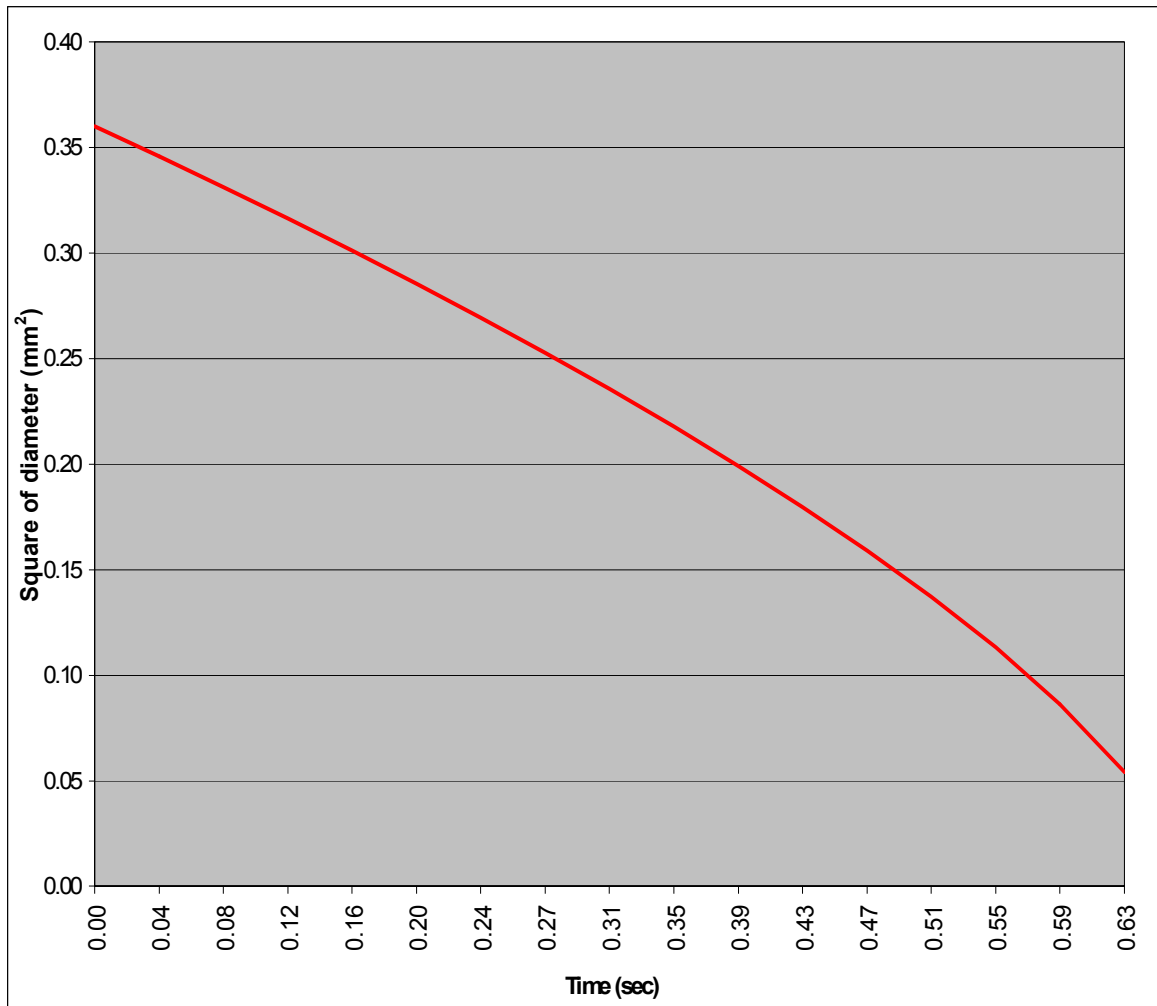


Fig. 5.1. Evaporation of stagnant gasoline droplet in quiescent ambient air.  $T_{\infty}=1000\text{K}$ ,  $P_{\infty}=1\text{bar}$ ,  $T_{w,0}=284\text{K}$ ,  $d_0=600\mu\text{m}$ .

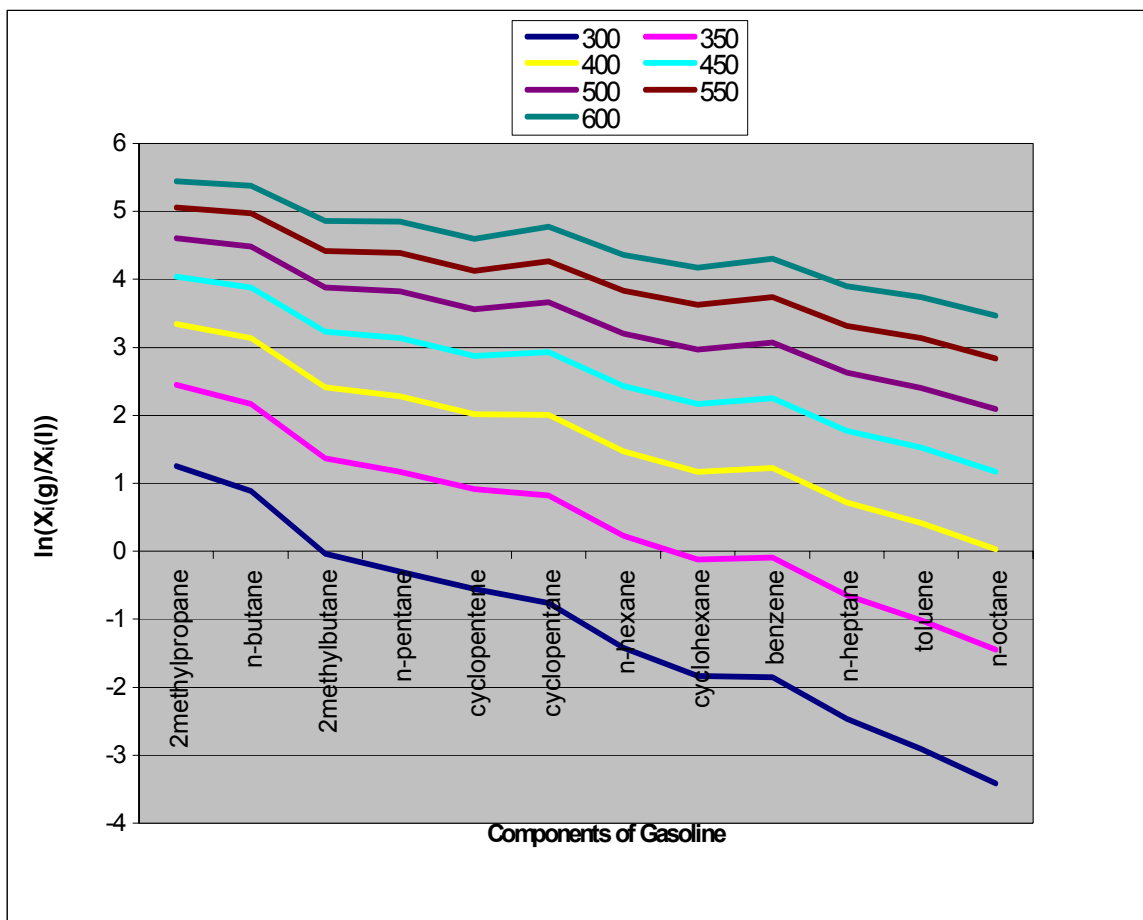


Fig. 5.2 Relative volatilities of components of gasoline droplet at different temperatures.

The model indicates preferential vaporization of the highly volatile light-end components as shown in Fig. 5.3.



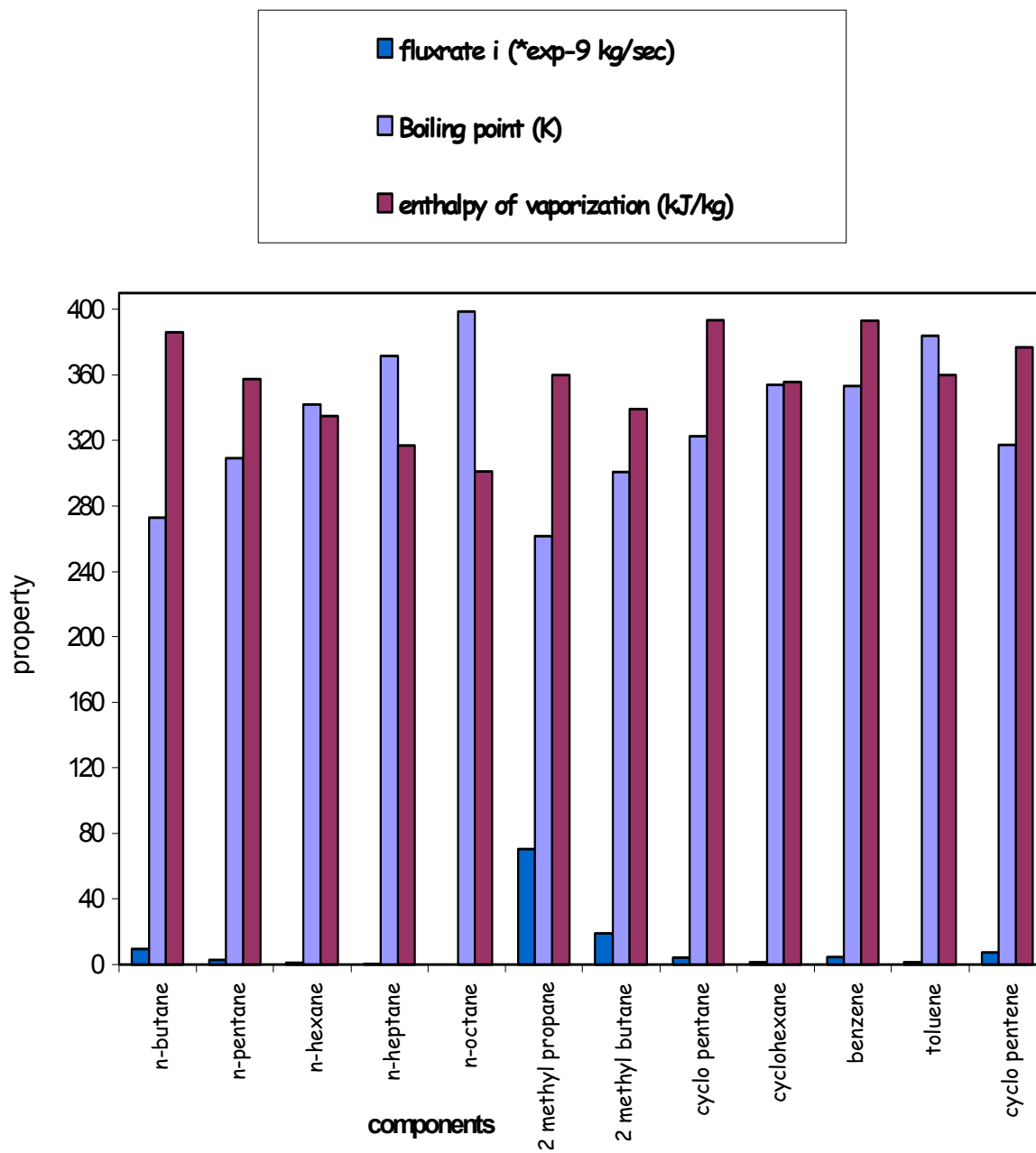


Fig. 5.3 Vaporization characteristics of individual species of gasoline droplet.

### 5.2.2 Diesel Droplet

The evaporation model described in the previous section was used to evaluate the variation of volatile molar fractions for a system of binary mixtures that represent diesel fuels as far as their volatility ranges are concerned. This binary system was chosen for investigation because experimental data was available from Randolph *et al.*<sup>17</sup> for the selected mixtures. Initial droplet heating period was not taken into account and the results are presented for steady and unsteady vaporization. Table 5.4 summarizes the thermo-physical properties (Chemnetbase<sup>21</sup>) of the individual hydrocarbons whose mixture in varying proportions signifies them as representative diesel fuels. The hydrocarbons chosen as representative of diesel fuels were binary mixtures of hexadecane with decane, hexadecane with dodecane, and hexadecane with tetradecane.

Table 5.4. Thermo-physical properties of hydrocarbons representative of diesel fuels

Component	W (kg/kmol)	L (kJ/kg)	T <sub>bp</sub> (K)
Decane(C <sub>10</sub> H <sub>22</sub> )	142.3	278.2	447.2
Dodecane(C <sub>12</sub> H <sub>26</sub> )	170.3	258.8	489.3
Tetradecane(C <sub>14</sub> H <sub>30</sub> )	198.4	242.8	526.6
Hexadecane (C <sub>16</sub> H <sub>34</sub> )	226.4	228.9	560.0

The diesel fuel investigation was split into three categories in the increasing order of volatility differentials. The relative volatilities of the components of the considered diesel droplet at various temperatures are shown in Fig 5.4. It can be inferred from the graph that decane is the most volatile and hexadecane, the least volatile among the droplets considered. The first mixture investigated was a binary droplet of hexadecane (designated by the symbol C<sub>16</sub>) and tetradecane (C<sub>14</sub>) and the other two investigated mixtures were hexadecane (C<sub>16</sub>) with dodecane (C<sub>12</sub>) and

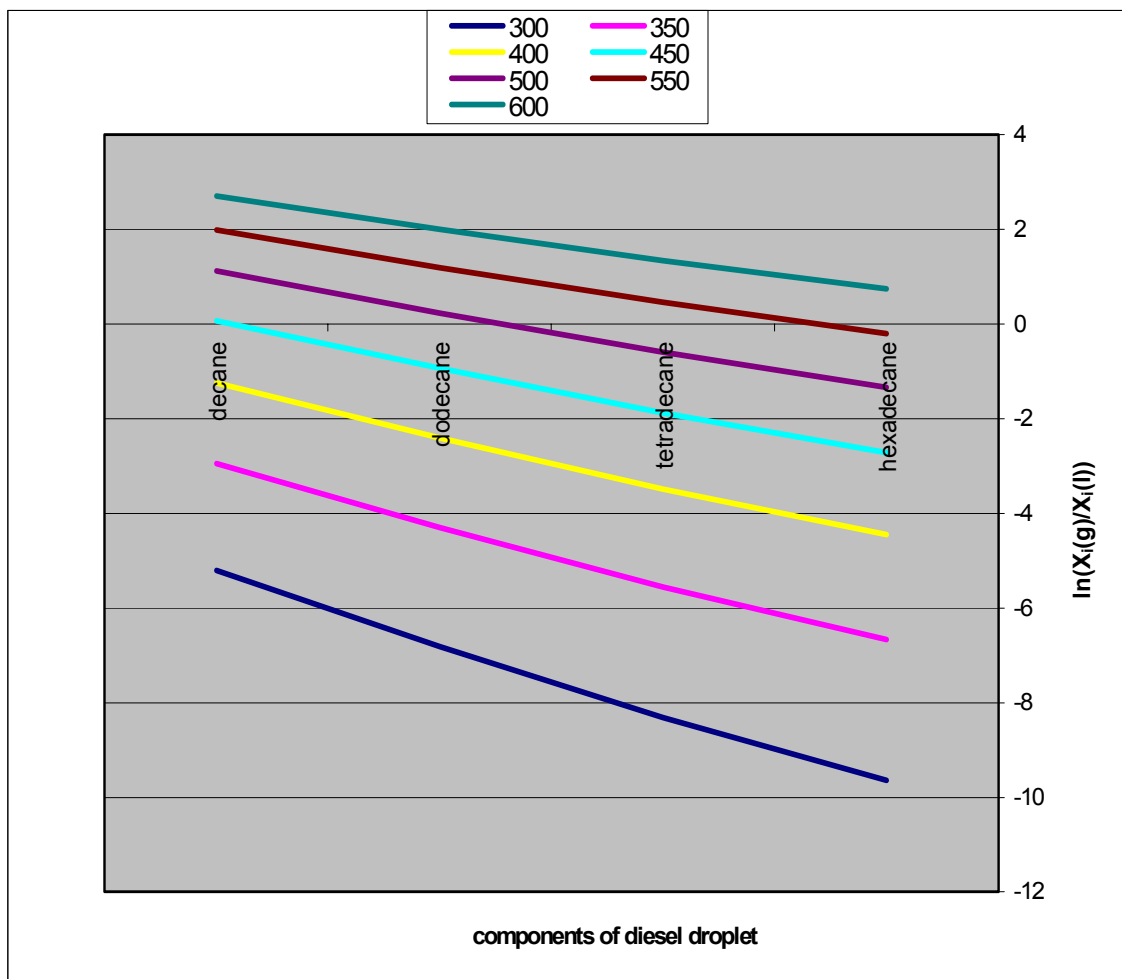


Fig. 5.4 Relative volatilities of components of diesel droplet at different temperatures.

hexadecane ( $C_{16}$ ) with decane ( $C_{10}$ ). Table 5.5 summarizes the input parameters used in the evaluation of diesel droplet evaporation characteristics.

Table 5.5. Table of input data for isolated diesel droplet evaporation

Fuel Diameter = 250 microns

**Ambient conditions**

Temperature ( $T_{\infty}$ ) = 1020K

Pressure ( $P_{\infty}$ ) = 1 bar

**Transport properties**

$c_p = 3.8$  kJ/kg-K

$\rho D (C_{16}/C_{14}) = 6.177 \cdot 10^{-5}$  kg/m-sec

$\rho D (C_{16}/C_{12}) = 5.58 \cdot 10^{-5}$  kg/m-sec

$\rho D (C_{16}/C_{14}) = 4.93 \cdot 10^{-5}$  kg/m-sec

Fig. 5.5 shows the variation of mass fraction in the liquid phase for the volatile component of the different mixtures mentioned above. With the instantaneous values for the droplet evaporation rate, flux ratios of species and the mass fractions of the species at the surface, the droplet size, concentration (in liquid phase), and temperature history are quantified. A less rigorous numerical techniques was utilized in the evaluation process in which the parameters were evaluated at time  $t=0$  and then marched to get the solutions at time  $t$ . The accuracy of the technique increases with decreasing step size. During the calculations, it was assumed that the droplet had an initial temperature corresponding to the steady state droplet temperature for the

given ambient conditions and initial mixture concentrations. The very purpose of using this temperature as the starting temperature for the droplet is to analyze the parameters with varying droplet composition rather than the transient heating effects.

The results presented correspond to an initial compositional fraction of 0.65, 0.6 and 0.55 respectively for the volatile component. Fig. 5.6 shows the square of droplet size as a function of time for the three cases. The curve is nearly a straight line indicating that at higher ambient temperatures wherein the droplet undergoes pure vaporization, the rate of vaporization follows the steady state pattern in that they are indifferent to changes in the droplet composition. The results indicate that as vaporization is initiated, the droplet remains at its initial temperature and the vaporization is dominated by the more abundant volatile component. The molar composition of the volatile component decreases monotonically and this would increase the droplet temperature which would reach a new steady state as the vaporization becomes more non-volatile component dominated. It is noted that at all times, the more volatile component is preferentially vaporized. If we invert the molar fractions making the mixture to be non-volatile dominant, still dodecane, tetradecane and decane which constitute the volatile fractions, would be preferentially vaporized. The only difference in this situation would be the rapid attainment of the transition to non-volatile evaporation regime.

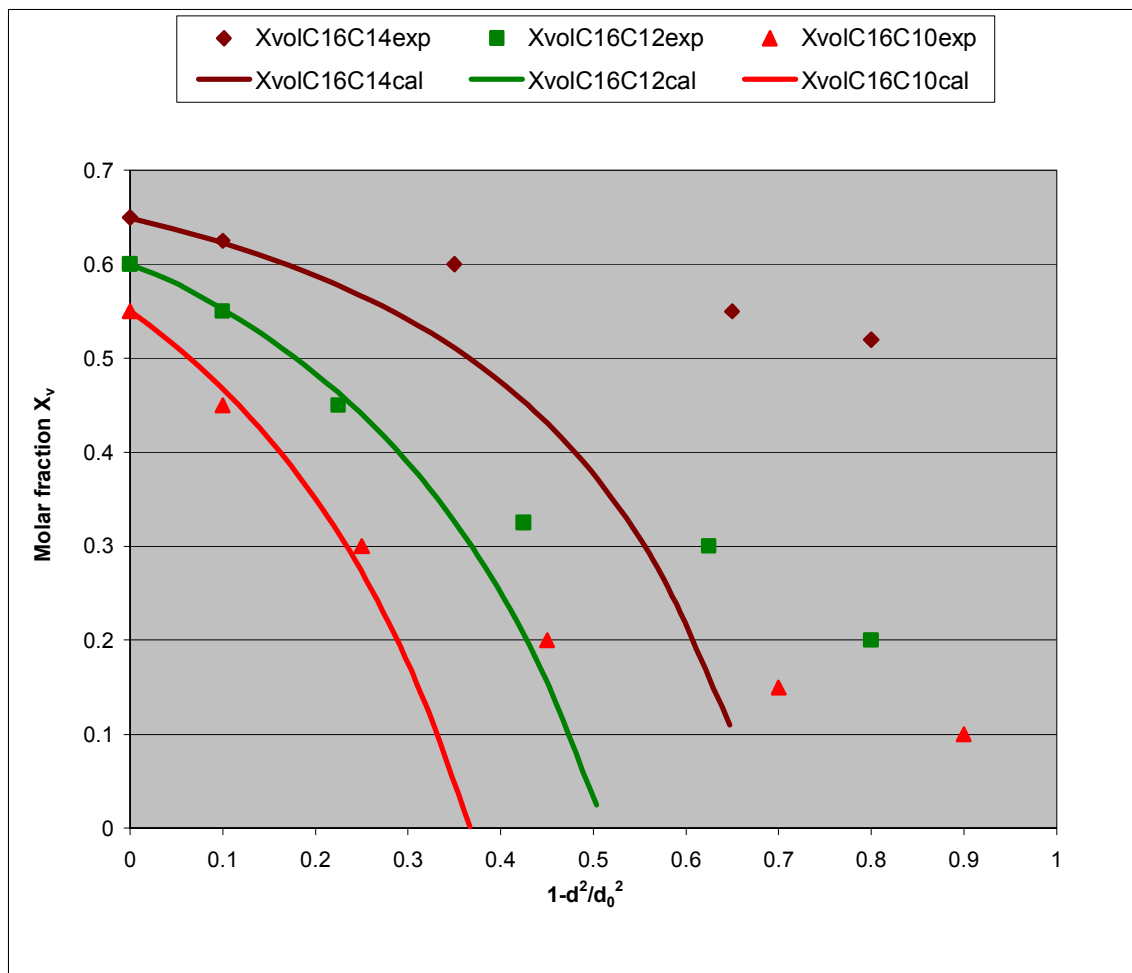


Fig. 5.5 Temporal variation of volatile molar fractions for mixtures of hexadecane with tetradecane, hexadecane with dodecane, and hexadecane with decane undergoing evaporation at 1020 K (initial droplet diameter is 245 microns).

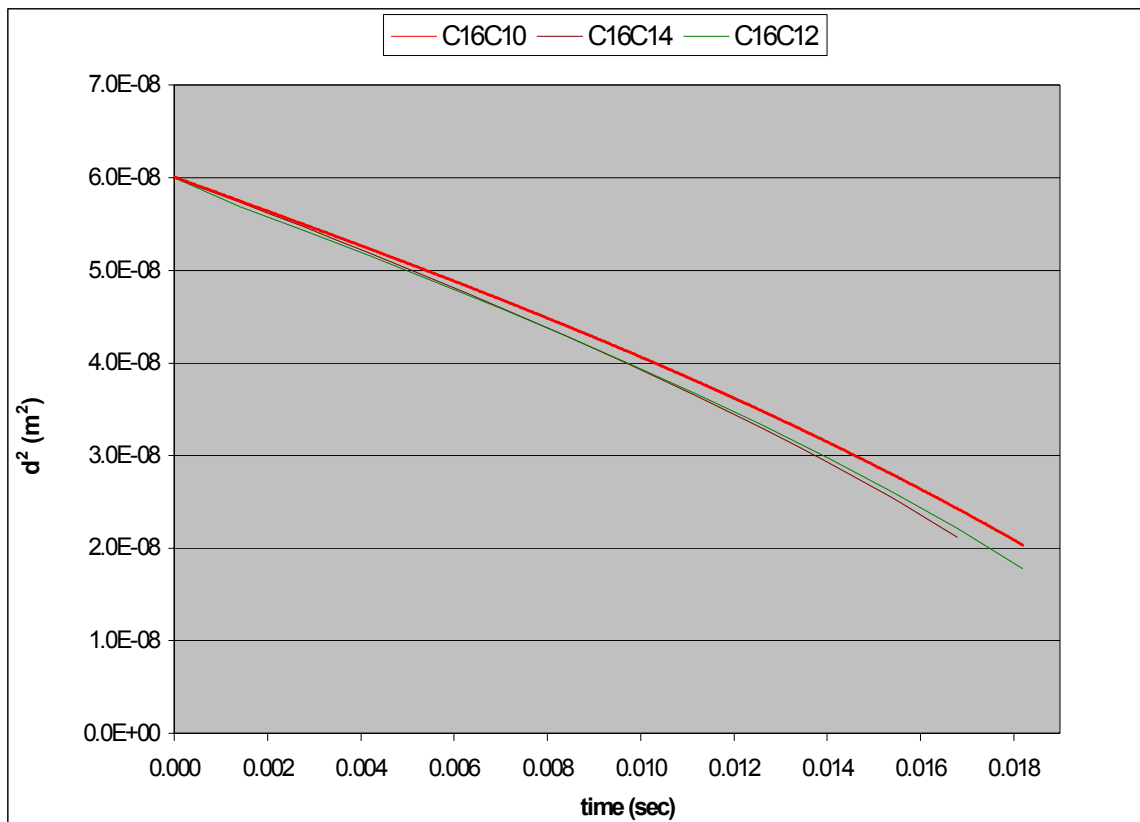


Fig. 5.6 Temporal variation of diameter for mixtures of hexadecane with tetradecane, hexadecane with dodecane and hexadecane with decane undergoing vaporization at 1020K.

The gas phase temperature and concentration profiles of the components of the diesel component were also studied. The temperature profiles of the three binary droplets are shown in Fig 5.7. It can be observed that the profiles attain a steady state as we move away from the droplet.

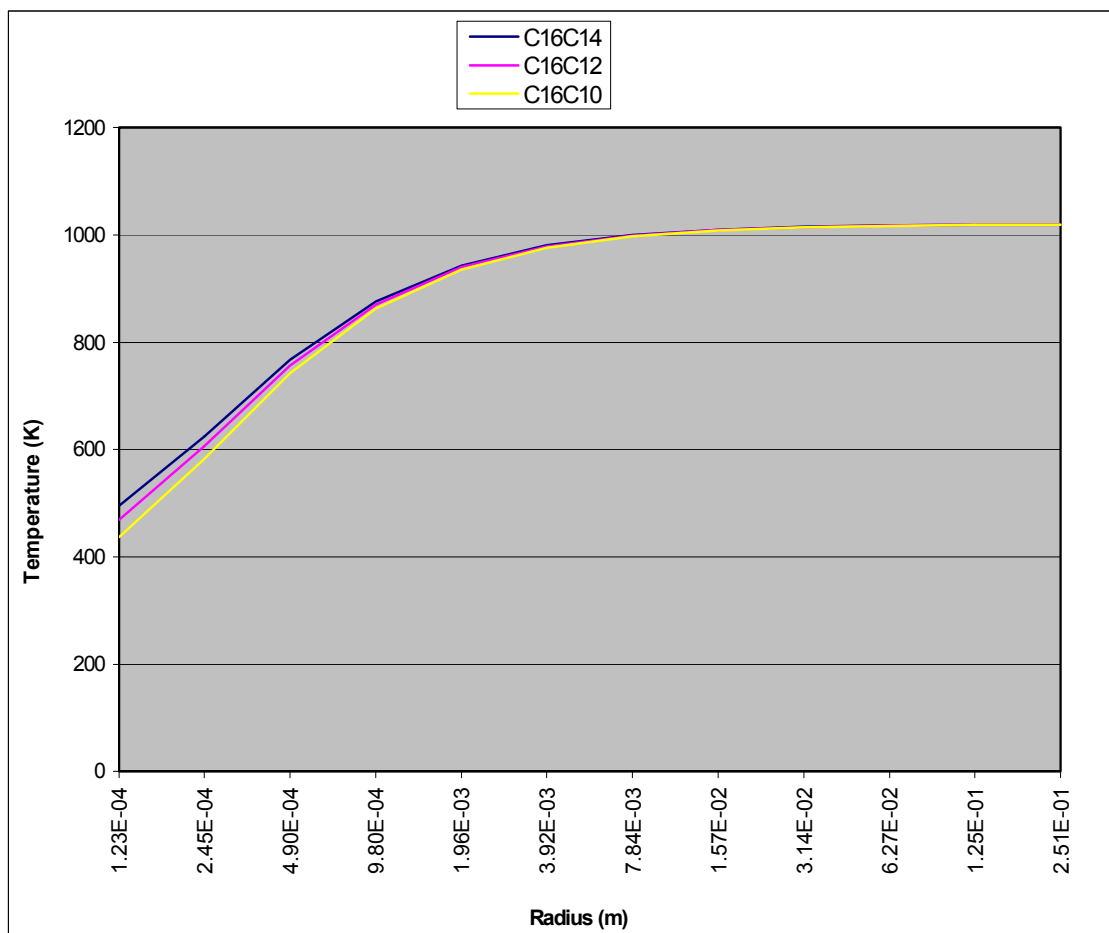


Fig. 5.7 Gas phase temperature profile for binary droplets of diesel undergoing vaporization at 1020K.  $d_0=1020\text{K}$ .

The concentration profiles of each of the binary droplets of hexadecane with tetradecane, hexadecane with dodecane and hexadecane with decane are shown in Figs. 5.8-5.10. The profiles indicate that the concentrations decrease as we move away from the droplet surface as expected. This is due to mass diffusion from the surface to the ambient and is dictated by the amount present at the wall surface.



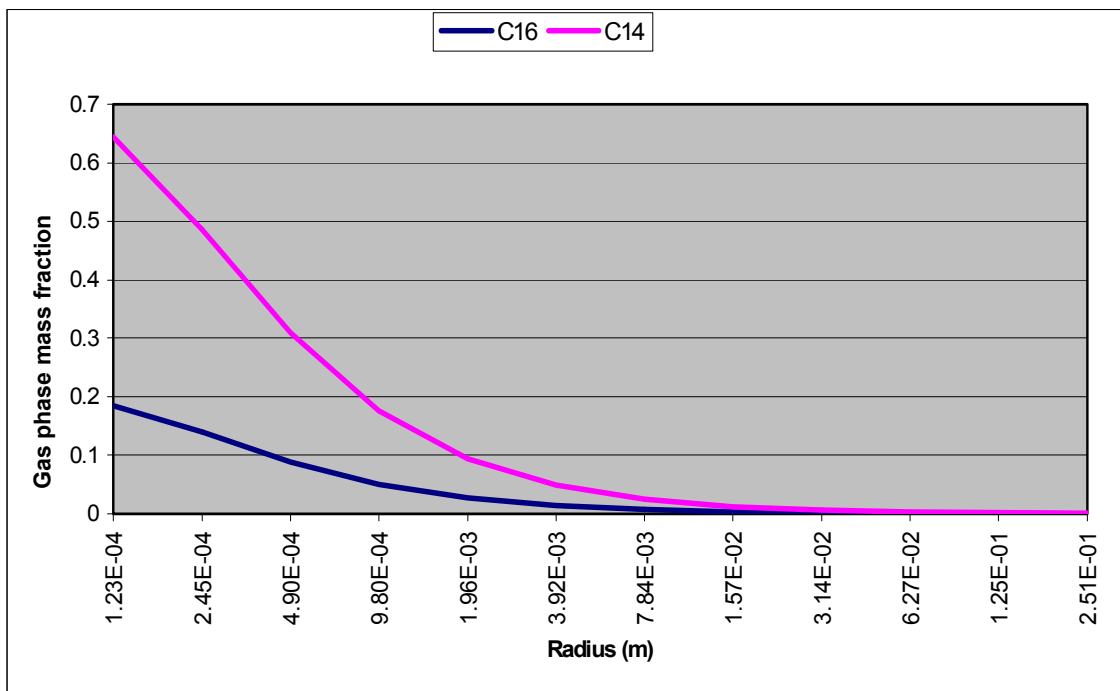


Fig. 5.8 Gas phase concentration profiles of binary droplet of hexadecane with tetradecane undergoing vaporization.  $T_{\infty}=1020\text{K}$ ,  $d_0=245\mu\text{m}$ .

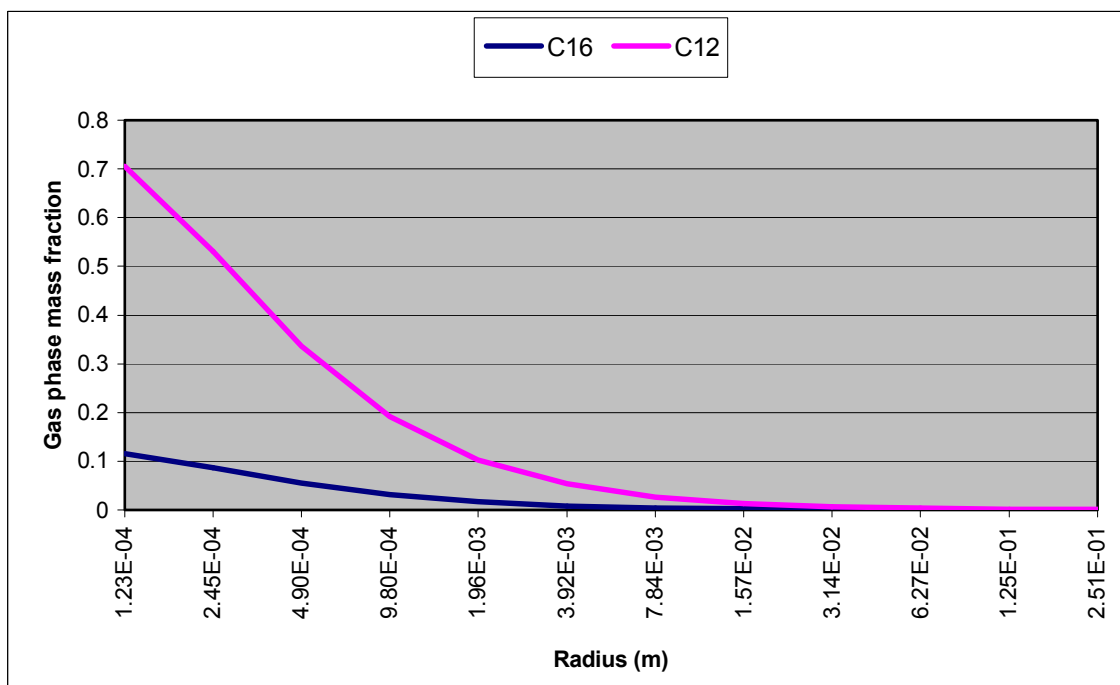


Fig. 5.9 Gas phase concentration profiles of binary droplet of hexadecane with dodecane undergoing vaporization.  $T_{\infty}=1020\text{K}$ ,  $d_0=245\mu\text{m}$ .

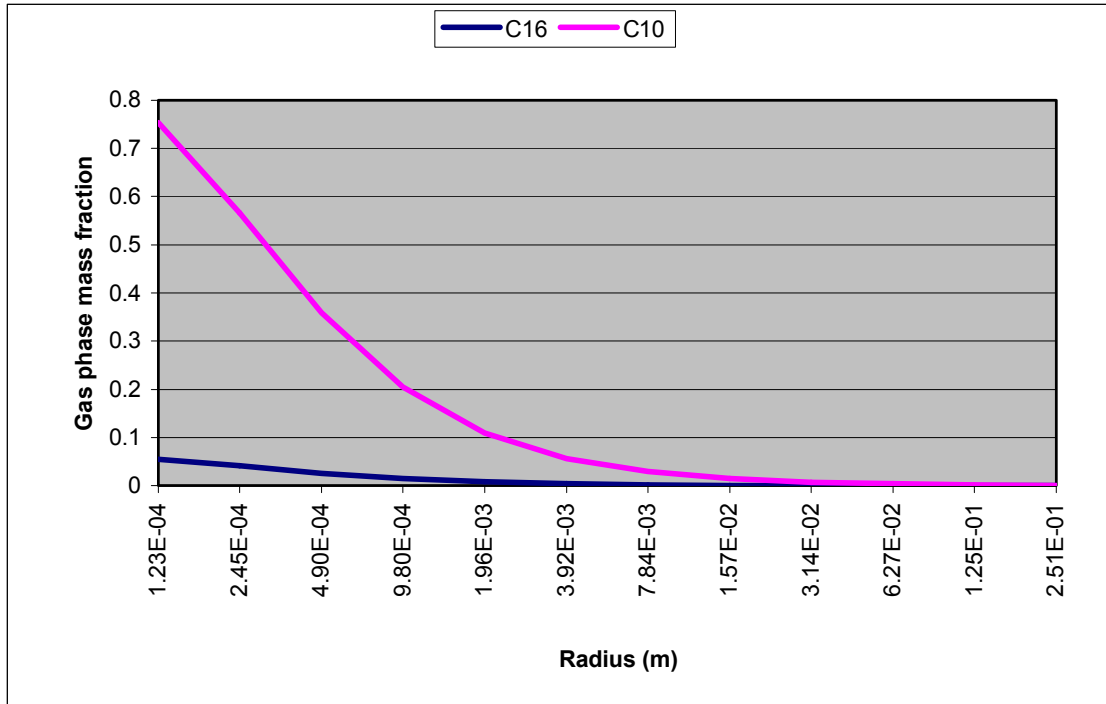


Fig. 5.10 Gas phase concentration profiles of binary droplet of hexadecane with decane undergoing vaporization.  $T_\infty=1020\text{K}$ ,  $d_0=245\mu\text{m}$ .

Fig. 5.11 shows the predicted history of droplet temperature for the three binary droplets discussed above at an ambient pressure of 1bar. These results incorporate unsteady vaporization model with the sensible latent heat of the droplet being considered. The variation of liquid phase mass fraction for the volatile components of the three binary droplets is shown in Fig. 5.12.

### 5.2.3 Comparison with Experimental Results

For the model calculations, the ambient was assumed to be at 1020K and the droplet diameter 245microns. The first point corresponds to the initial state when vaporization is initiated. It can be observed from experimental evidence that while  $C_{16}/C_{14}$  droplet seems to behave in a steady state manner, for the  $C_{16}/C_{12}$  and  $C_{16}/C_{10}$  droplet, the concentration of the more volatile component, namely dodecane and decane continuously decreases.

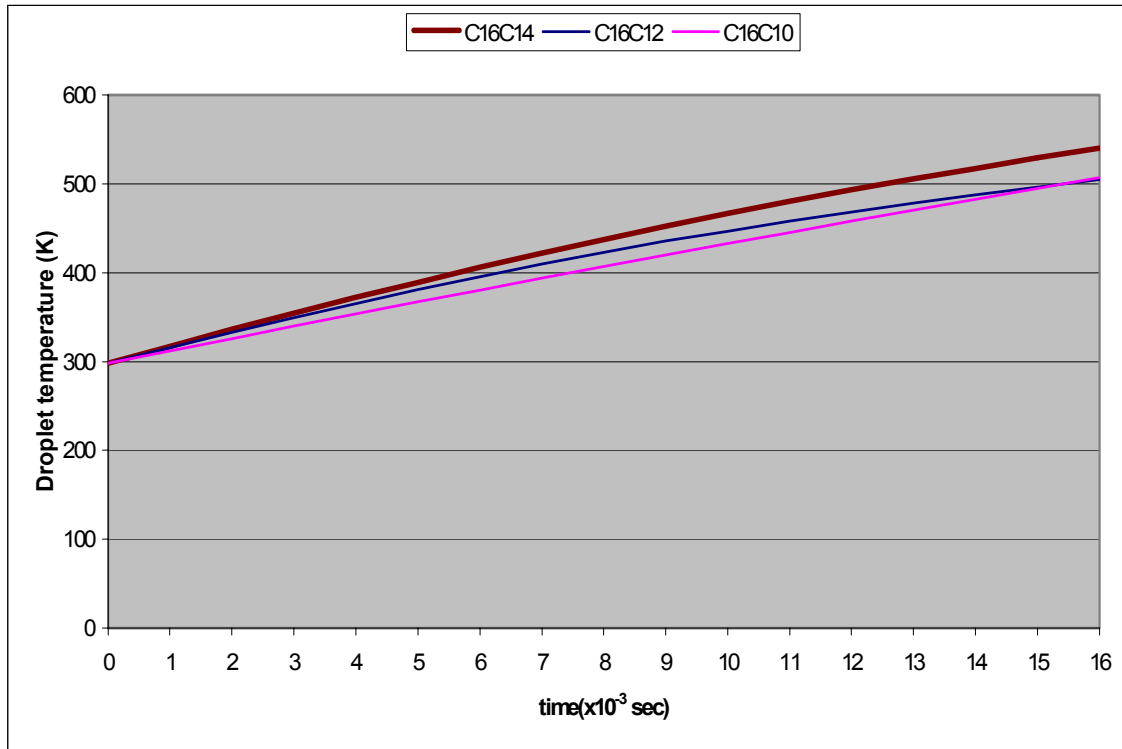


Fig. 5.11 Temporal behavior of temperature of binary droplets of diesel undergoing unsteady vaporization.  $T_{\infty}=1020\text{K}$ ,  $d_0=245\mu\text{m}$ .

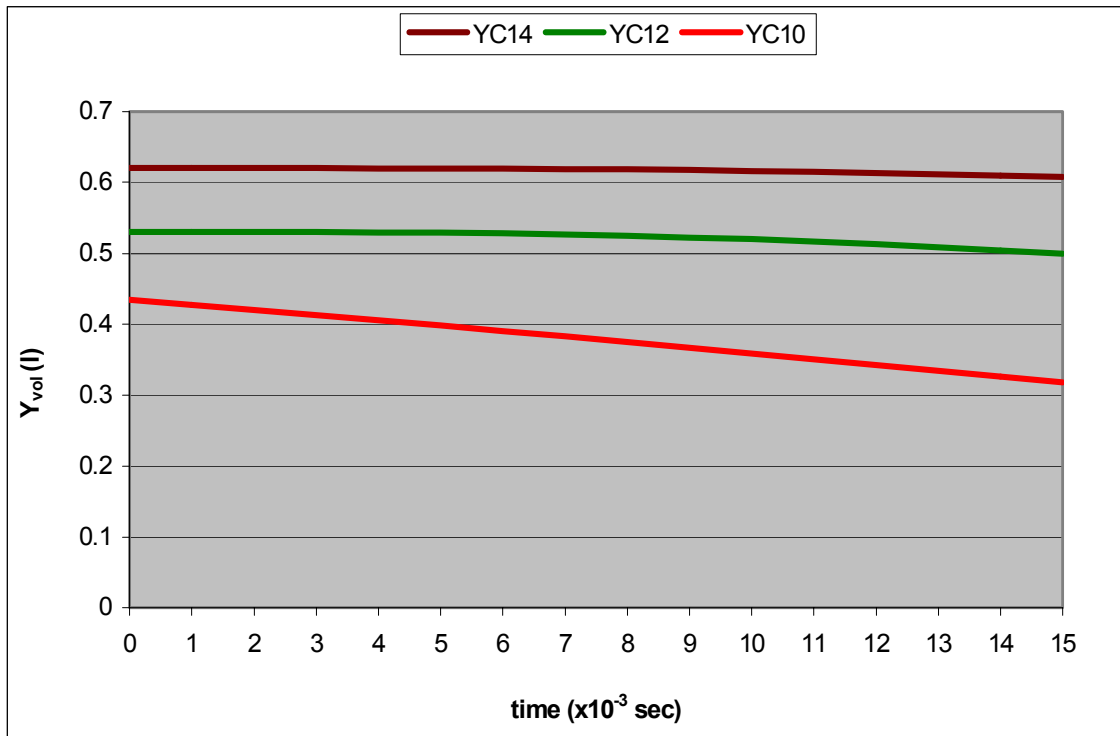


Fig. 5.12 Temporal variation of volatile component mass fraction of diesel droplets undergoing unsteady vaporization.  $T_{\infty}=1020\text{K}$ ,  $d_0=245\mu\text{m}$ .

behave in a steady state manner, for the  $C_{16}/C_{12}$  and  $C_{16}/C_{10}$  droplet, the concentration of the more volatile component, namely dodecane and decane continuously decreases. The experimental evidence seems to indicate the influence of liquid phase mass diffusivity. The liquid phase diffusivity was also calculated theoretically by Randolph *et al.*<sup>17</sup> using an approximate expression similar to the one described by Reid and Sherwood<sup>24</sup>. The fuel blends with increased volatility differential seem to possess higher mass diffusivity resulting in lesser liquid phase diffusional resistance. The mass diffusion coefficient depends on the reduced mass of the species and hence lighter the species, higher the mass diffusivity.

### 5.3 COMBUSTION RESULTS

The double Shvab-Zeldovich formulation explained in the previous section to model multicomponent droplet combustion was applied and validated against experimental data and the results are presented in this section. The model was first validated against a binary component droplet initially consisting of 50% undecane and 50% octanol by volume. The burn rate constant predicted from theory was validated against experimental data available from Law and Law<sup>16</sup>. The model was then applied to diesel-fuels represented by the hydrocarbons explained in the previous section in the same proportion in the liquid phase. The results from the model were then validated against and compared with the available experimental data from Randolph *et al.*<sup>17</sup>.

#### 5.3.1 Octanol-Undecane Droplet

The binary components selected for the initial validation were octanol and n-undecane, which have identical boiling points at atmospheric pressure. Their thermo-physical properties are summarized in Table 5.6. Law and Law<sup>16</sup> had earlier demonstrated the existence of  $d^2$ -law for these multicomponent droplets. It is against these results that the current model was validated. The choice of the droplet was based on the necessity to reduce internal bubbling (Law<sup>25</sup>) and pre-vaporization before ignition. The volatility of the droplet selected accounts for minimum compositional variation and minimal droplet heating. These criteria serve as assumptions for our model.

Table 5.6. Thermo-physical properties of octanol and n-undecane

Component	W(kg/kmol)	L(kJ/kg)	T <sub>bp</sub>	h <sub>c</sub> (kJ/kg)	u <sub>o2</sub>
Octanol	130.2	388.3	467.5	40651	2.954
n-undecane	156.3	265	469	47540	3.487

The combustion of a binary component droplet was investigated in an environment having a pressure of 1atm and  $X_{o,\infty}=0.4$ . The ambient temperature was taken as 1000K and the droplet radius 470microns. In Fig. 5.13, the experimental data for the burn rate constant is compared with that from the theoretical curve. The burn rate constant evaluated through the model was  $1.17\text{mm}^2/\text{sec}$  and that from experiments was  $0.952\text{mm}^2/\text{sec}$ . The curve does not show the droplet heating time, which might span about 10-15% of the droplet lifetime. The rates of vaporization of the two droplets are more or less the same due to identical volatilities and hence it might be reasonable to predict a steady state temperature. It is clear that the theoretical curve compares well with the experimental data.

### 5.3.2 Diesel Droplet

The experimental results of Randolph *et al.*<sup>17</sup>, all on binary droplets representative of diesel fuels in their volatility ranges were used as a test of validation for the combustion parameters evaluated using the present model. All the results presented here are for the pure combustion of three different binary droplets with the ambient at 1300K. For combustion calculations, the gas phase specific heat was taken as 2.5 kJ/kg-K. The gas phase properties are representative of those of the mixture consisting of fuel vapor and ambient gas between  $T_w$  and  $T_\infty$ . The initial droplet diameter was taken as 255 $\mu\text{m}$ . Fig. 5.14 shows the molar concentration profiles (non-dimensional) of the volatile component, namely decane, dodecane and tetradecane in the mixture. In Fig. 5.14, the first point corresponds to the state when ignition has just been achieved. The curve from the model shows that for all the three binary droplets, the concentration of the more volatile component in the mixture continuously decreases.

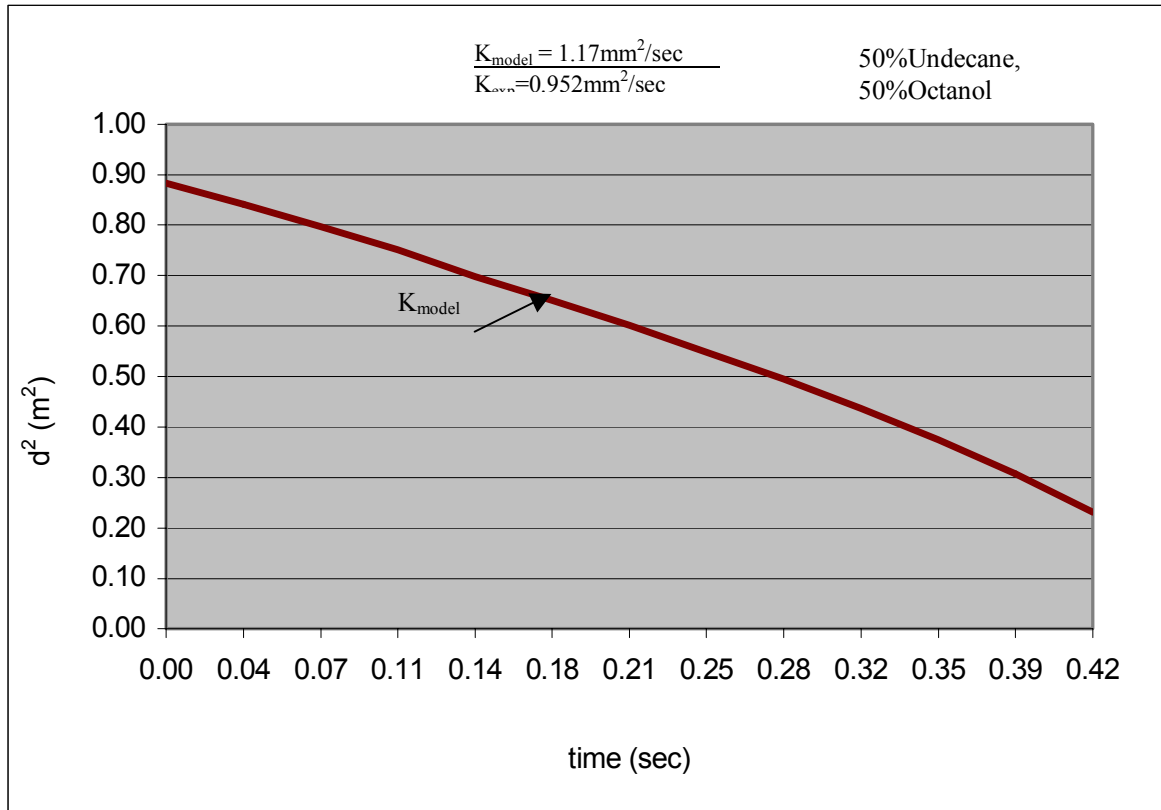


Fig 5.13 Comparison of model and experimental burn rates of a binary droplet of octanol and undecane.  $T_{\infty}=1000\text{K}$ ,  $d_0=940\mu\text{m}$ .

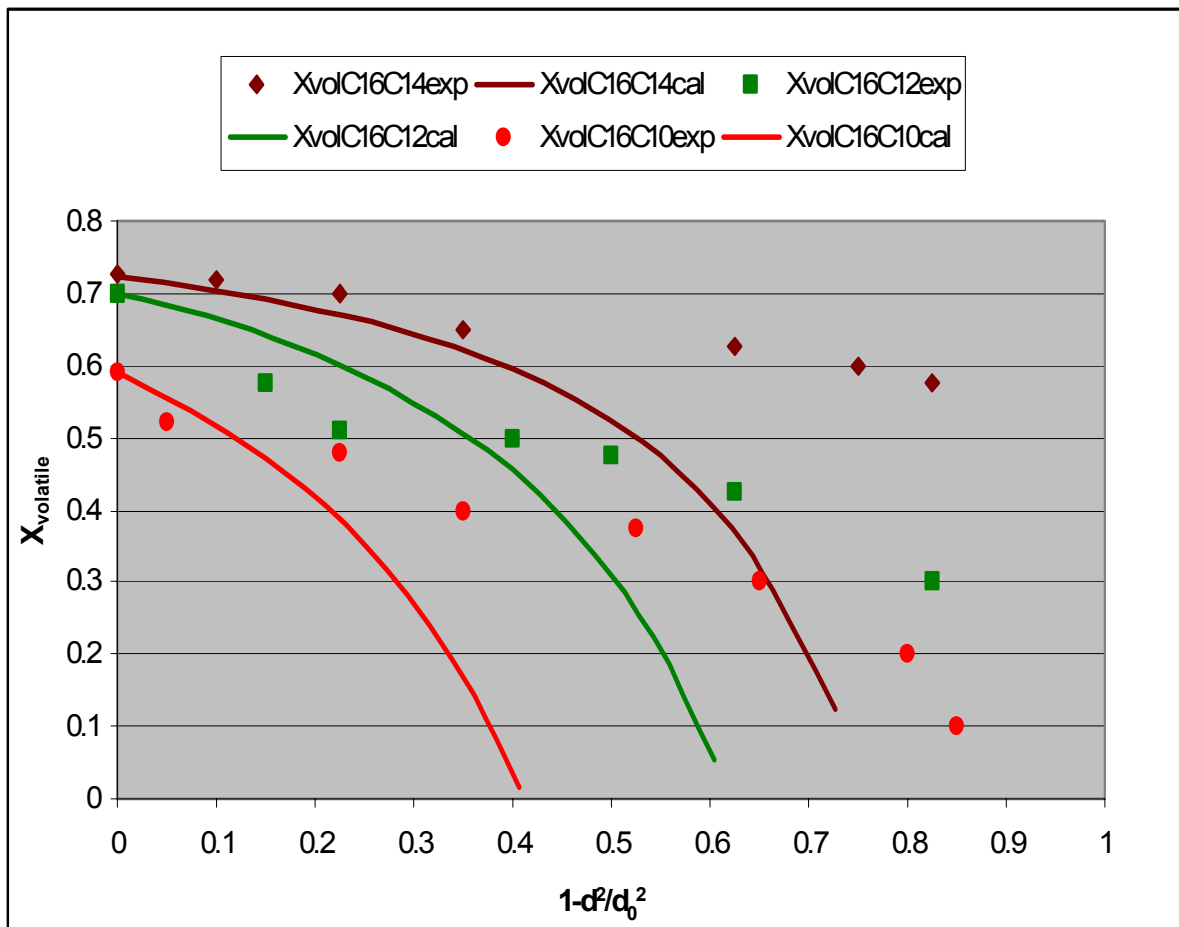


Fig 5.14 Temporal variation of volatile molar fractions for binary mixtures of hexadecane with tetradecane, hexadecane with dodecane, and hexadecane with decane, undergoing combustion at 1300K (initial droplet diameter is 255 $\mu$ m).



Fig. 5.15 shows the variation of square of the droplet diameter with time. The calculated property values are tabulated in Table 5.7 for the droplets.

Table 5.7. Calculated property values for the binary droplets representative of diesel fuels

Mixture	$\rho D$ ( $\times 10^{-5}$ ) (kg/m-sec)	$h_{c,O2}$ (kJ/kg)
C <sub>16</sub> /C <sub>14</sub>	9.917	13644
C <sub>16</sub> /C <sub>12</sub>	8.673	13626
C <sub>16</sub> /C <sub>10</sub>	7.378	13627

The gas phase temperature and concentration profiles of the components of the diesel component undergoing combustion was also studied. The temperature profiles of the three binary droplets are shown in Fig 5.16. It can be observed that the temperature in the gas phase increases as we move towards the flame radius. The gas phase temperature is maximum at the flame where there is stoichiometric combustion of the species. As we move away from the flame towards the ambience, the gas phase temperature decreases till becomes equal to the ambient temperature.

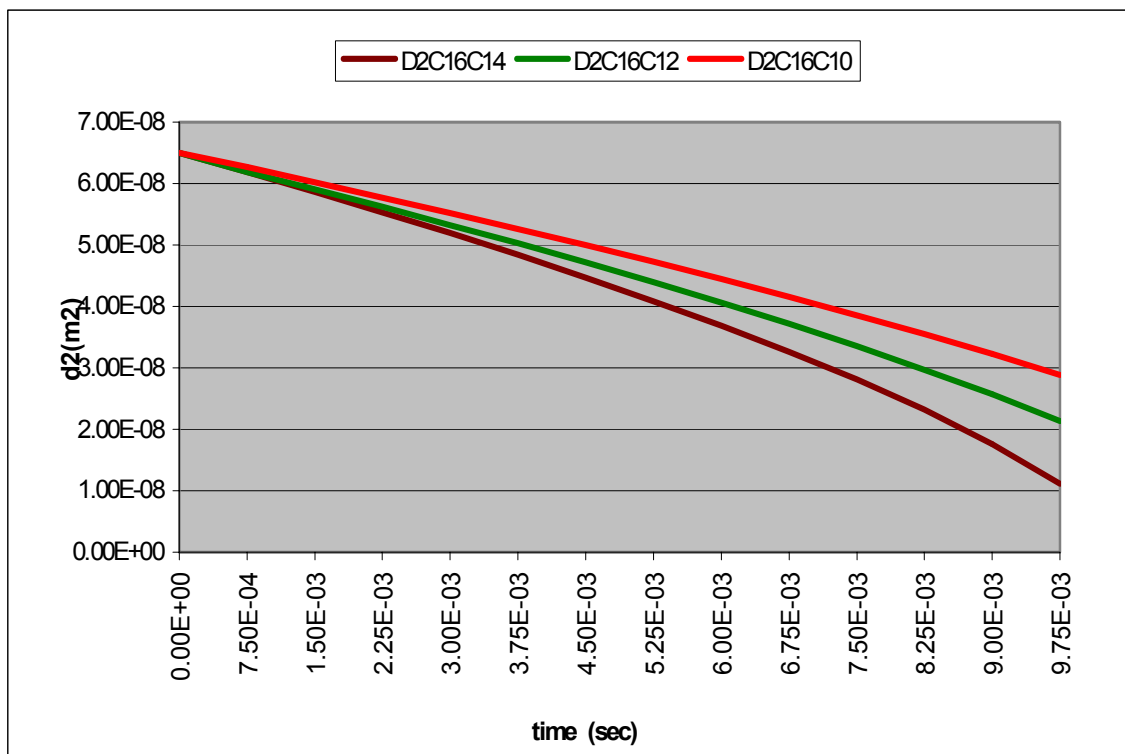


Fig. 5.15 Temporal variation of diameter for mixtures of hexadecane with tetradecane, dodecane and decane undergoing combustion at 1300K.  $d_0=255\mu m$ .

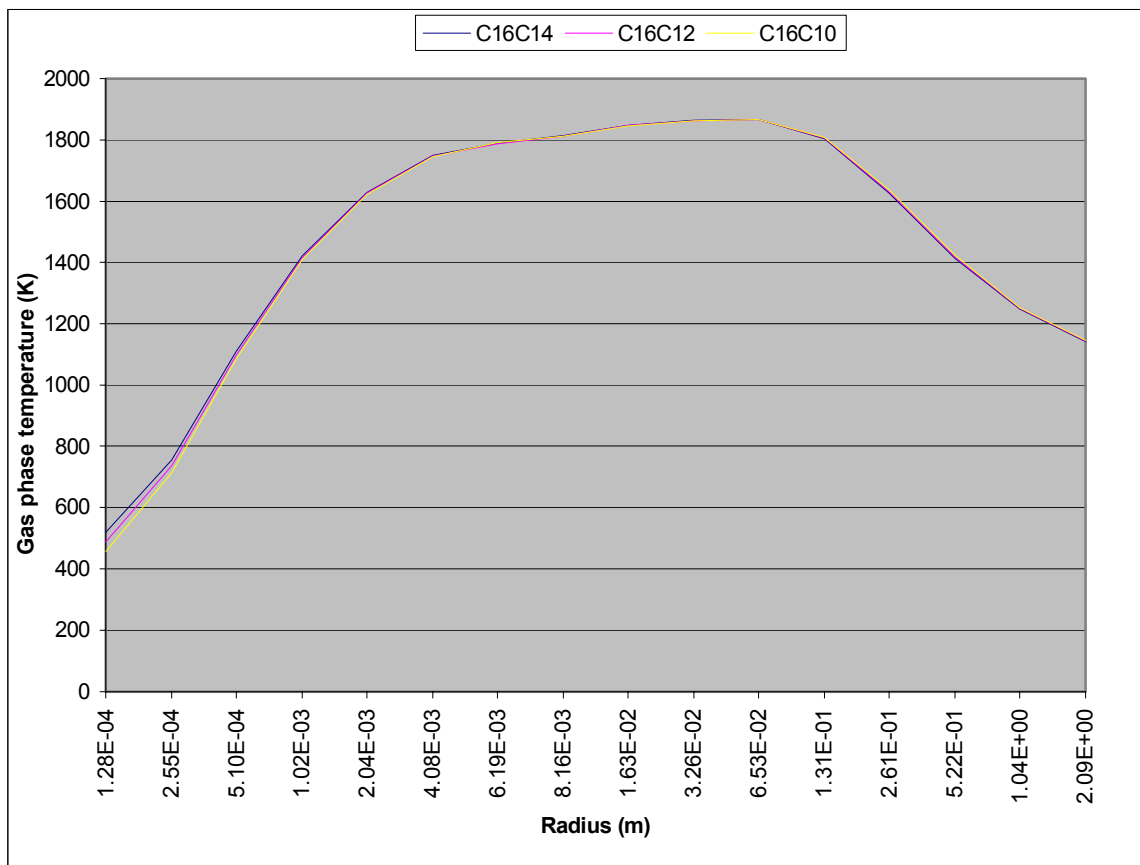


Fig. 5.16 Gas phase temperature profiles for binary droplets of diesel undergoing combustion.  $T_{\infty}=1300\text{K}$ ,  $d_0=255\mu\text{m}$ .

The concentration profiles in gas phase of the individual species of the binary diesel droplet undergoing combustion are shown in Figs. 5.17-5.19. The profiles indicate that the concentrations decrease as we move away from the droplet surface and reduce to zero at the flame radius where it is completely consumed by the oxidizer species. The profile of the oxidizer species is also shown in the figure. It can be observed that the oxidizer gets completely consumed at the flame radius as expected.

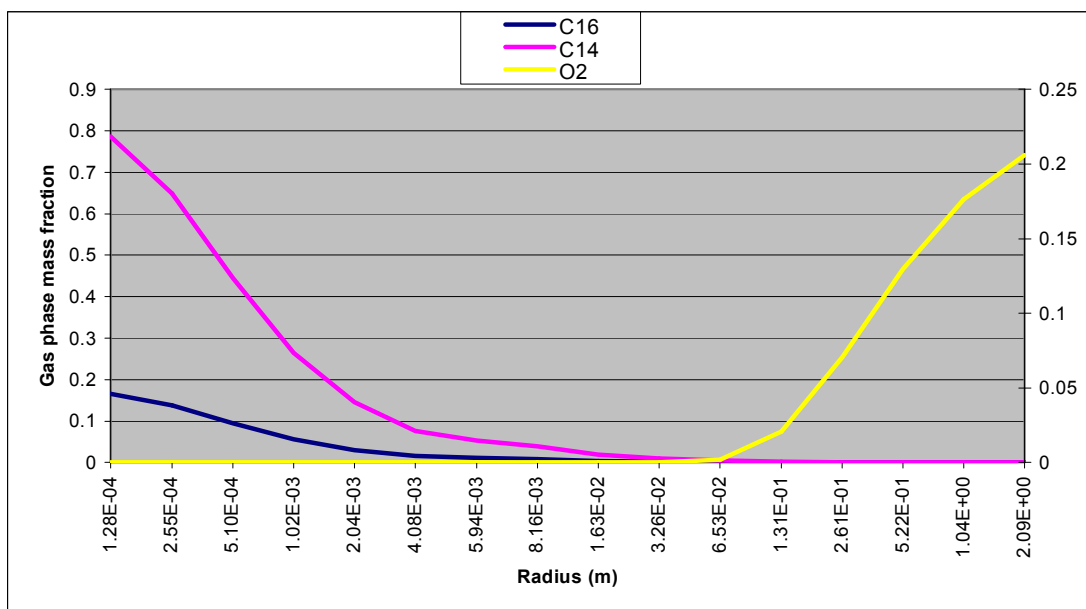


Fig. 5.17 Gas phase concentration profiles of oxygen, hexadecane and tetradecane for a binary droplet of hexadecane and tetradecane undergoing combustion.  $T_{\infty}=1300\text{K}$ ,  $d_0=255\mu\text{m}$ .

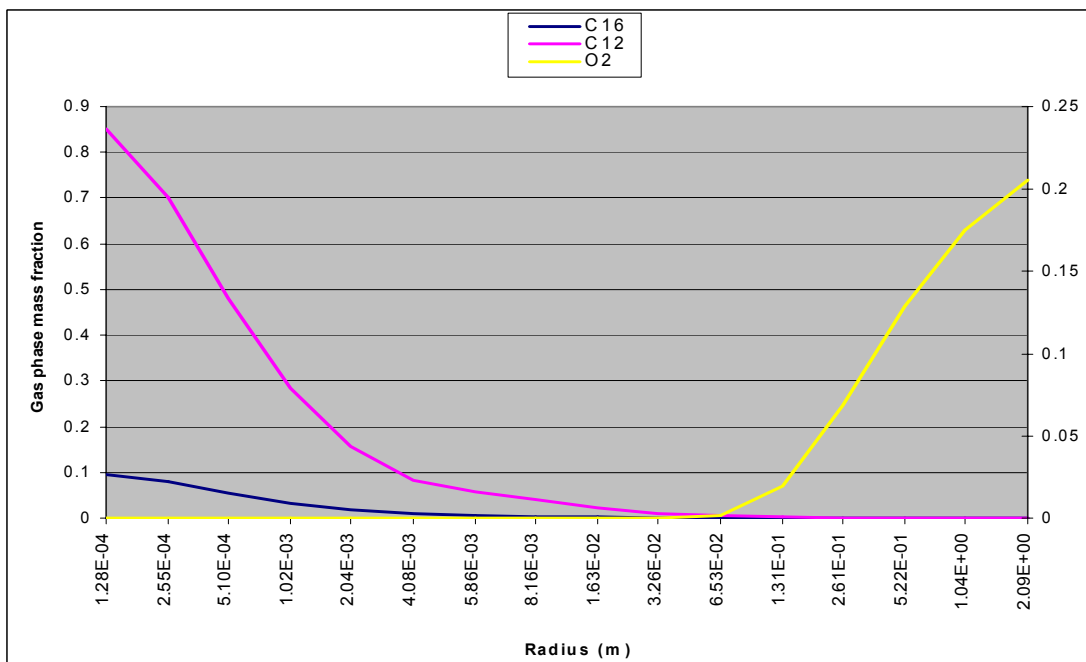


Fig. 5.18 Gas phase concentration profiles of oxygen, hexadecane and dodecane for a binary droplet of hexadecane and dodecane undergoing combustion.  $T_{\infty}=1300\text{K}$ ,  $d_0=255\mu\text{m}$ .

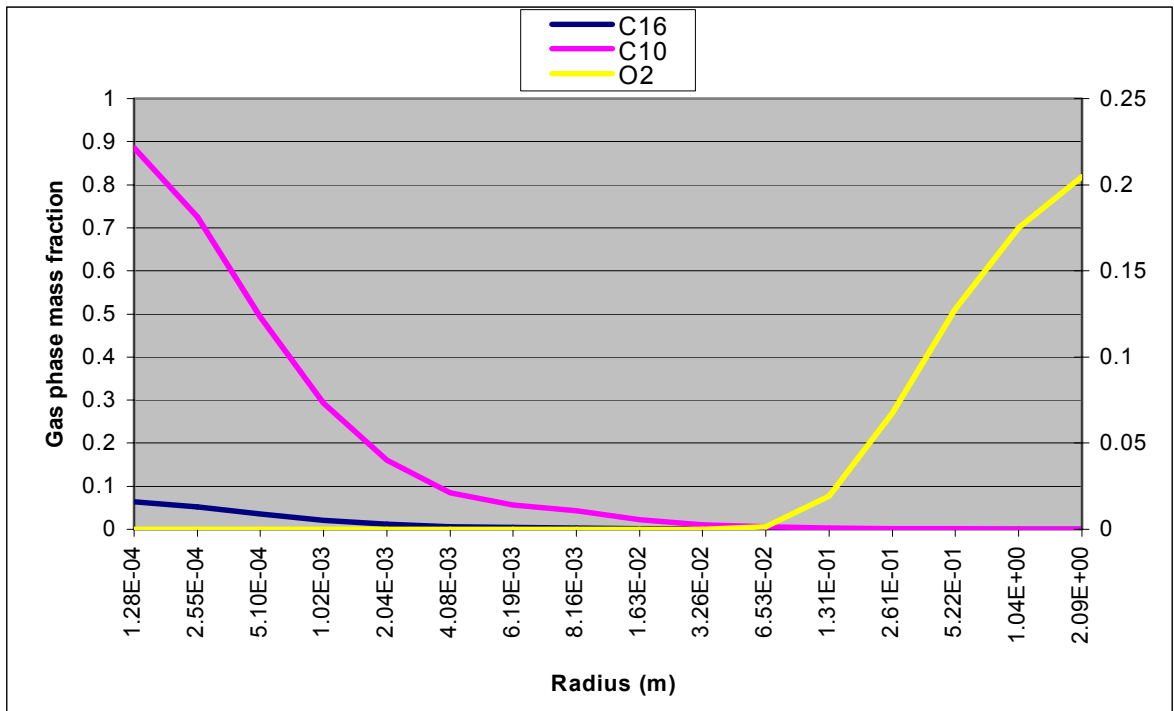


Fig. 5.19 Gas phase concentration profiles of oxygen, hexadecane and decane for a binary droplet of hexadecane and decane undergoing combustion.  $T_{\infty}=1300\text{K}$ ,  $d_0=255\mu\text{m}$ .

### 5.3.3 Comparison with Experimental Results

The experimental results as seen from Fig 5.14 seem to indicate a strong influence of liquid phase mass diffusion. Hence, this model serves as a good source to test the assumption if internal circulation is sufficiently strong for these droplets. Fig. 5.14 strongly seems to show that as the properties continuously change, the concentration continuously changes and attains a steady state only after the volatile component has been completely vaporized and the droplet is left with one component. The result from the model (continuous line) varies from the experimental data values (data points) in that the experimental values suggest steady state variation for the deviation of the mixture with lesser volatility differential. The experimental behavior once again seems to

indicate the role of liquid phase mass diffusivity. Since the gasification rate for burning is dominant compared to the case of evaporation, the slope indicates a longer time available for diffusion in the case of evaporation.

## **6. SUMMARY AND FUTURE WORK**

### **6.1 SUMMARY**

The spherically symmetric combustion of a single, isolated fuel droplet continues to be a viable configuration in which to study fundamental liquid combustion phenomena. The results presented in this thesis serve as approximate solutions through a simple formulation to analyze combustion problems of multicomponent fuels. Unfortunately, there is lack of available experimental data to validate the results as applied to transportation fuels of the likes of gasoline and diesel probably due to complex phenomena within liquid phase during combustion. The validation of the model has been attempted and has proven successful against available experimental data involving binary droplets. The double Shvab-Zeldovich formulation developed for binary mixture can be applied to any multicomponent fuel to determine its combustion characteristics. The major results from the thesis are summarized here along with possibilities for continued research in droplet combustion and other related areas.

#### **6.1.1 Gasoline Droplet Evaporation Results**

The evaporation results indicate preferential vaporization of highly volatile light-end components in gasoline. The results indicate that gasoline droplets do not reach a steady drop temperature as in the case of single-component droplets. This is because the droplet composition continuously changes with preferential vaporization of volatile components. Droplet temperature and concentration profiles are not plotted for lack of experimental data available on gasoline for validation. However theoretical results are presented. Droplet lifetime predicted by the model assumes that droplet temperature is uniform while interior temperature could be different compared to surface temperature during heating process, particularly for a large drop. It is found that the droplet surface area decreases gradually with time from the beginning and the

evaporation constant is  $0.344 \text{ mm}^2/\text{sec}$  in close agreement with the results from the evaporation model of Ra and Reitz<sup>26</sup>.

### 6.1.2 Diesel Droplet Evaporation Results

By incorporating the multicomponent evaporation formulation developed by Annamalai *et al.*<sup>2</sup>, evaporation of representative diesel fuels were modeled. Binary droplets with mixtures of hexadecane with tetradecane, dodecane, and decane were taken to be representative of diesel fuels considering their volatility ranges.

The decrease of diameter-square with time is found to be linear. This resembles steady state behavior of droplet wherein the rate of vaporization is invariant to changes in droplet mixture composition. This is attributed to the high surrounding temperature to which the droplet is exposed. The numerical results for the validation of liquid phase concentration of the more volatile component within an individual binary droplet reproduce the qualitative results of the experiments by Randolph *et al.*<sup>17</sup> wherein the mixtures diffuse internally inside the droplet. The results indicate that the extent of volatility differential and mass diffusivity of the droplet affect the liquid phase diffusional resistance. The model results show that the volatile component composition continuously decreases due to its preferential vaporization from the surface. Since the model does not incorporate liquid phase diffusion into it, the quantitative differences are expected.

### 6.1.3 Octanol-Undecane Droplet Combustion Results

The combustion model that has been formulated in this thesis is validated using the experimental results of Law and Law<sup>16</sup> for a binary alcohol-alkane droplet of octanol and undecane. The burn rate obtained using the present double Shvab-Zeldovich formulation was  $1.17 \text{ mm}^2/\text{sec}$  which compared well with that obtained experimentally by Law and Law<sup>16</sup>. The experimental data is based on the condition that droplet is not subjected to rapid internal motion.



In other words, experimental conditions were set up such that the combustion was liquid-phase diffusion controlled. This is different from the assumption of the present model, which assumes perfect mixing inside the model, i.e. more internal circulation to keep temperature uniform. The burn rates agree well qualitatively. The slightly higher burn rate is attributed to the internal circulation through which the volatility differentials exert a higher influence on the burning behavior. Based on the validation of this value of burn rate, the formulation is then extended to model the combustion of diesel like fuels mentioned in the previous section.

#### **6.1.4 Diesel Droplet Combustion Results**

The multicomponent combustion model was applied to mixtures of  $C_{16}$  with  $C_{14}$ ,  $C_{12}$ , and  $C_{10}$ . The experimental data indicates that the concentration of the more volatile component deviates from steady state behavior with increasing volatility differential. This behavior seems to indicate the existence of liquid phase mass diffusivity. The theoretical model shows continuous decrease in the concentration profiles of the volatile components. The trend matches qualitatively with the experimental profile.

The combustion model described in this thesis does not account for liquid phase mass diffusion and hence the effect of liquid phase Lewis number is neglected on the droplet gasification behavior. The available experimental data suggests that the gasification behavior is intermediate to those of distillation and diffusion limited steady state whereas the calculations suggest more of batch distillation behavior. A direct implication of the presented results is that with rapid internal mixing, there would be no question of entrapment of the volatile components interior of the droplet leading to nucleation and further atomization.

## **6.2 FUTURE WORK**

The results presented and summarized in this thesis paves the way for further research in few directions. Potential research areas may include new multicomponent experiments, additional numerical modeling and study of droplet interior.

### **6.2.1 Multicomponent Experiments**

The results presented in this thesis for evaporation of gasoline assumes gasoline to be made of discrete hydrocarbon fractions of fixed composition. In reality, gasoline, a petroleum distillate, comprises of more than 250 hydrocarbon species. Hence, it is desirable to device experiments to measure the combustion stages of volatile fuels like gasoline, diesel and kerosene. It is worth mentioning nevertheless that for volatile fuels of the likes of gasoline, it is difficult to achieve measurements of the combustion stages at rigorously well-defined conditions (Ra<sup>27</sup>). It is a challenge to design such an experiment and validate data of models. Through these experiments, it is also possible to validate if the multicomponent combustion of droplet of the likes of gasoline holds the assumptions of the model in good stead. It could serve as a good source to identify the gasification behavior.

### **6.2.2 Droplet Combustion Modeling**

Additional droplet evaporation and combustion models have to be developed which takes into account liquid phase diffusion. Currently, the evaporation models formulated to understand multicomponent evaporation characteristics of gasoline (Ra and Reitz<sup>26,28</sup>) and kerosene (Harstad and Bellan<sup>29</sup>) utilize the method of continuous thermodynamics to model these multicomponent fuels. Including liquid phase diffusion of droplet in these models might give a better idea on droplet behavior in the absence of internal mixing and prove to be a better platform for experimental validations.

As the ambient temperature increases, the results become sensitive to the variations in the transport properties. The present and available models use constant transport properties in the gas phase assuming a Lewis number of unity. The evaporation and combustion characteristics can be more accurately predicted by developing a model, which incorporates into it the transport property variations of each species in the gas phase.

### **6.2.3 Study of Droplet Interior**

There has been considerable dispute with regards to what is happening to the species inside the droplet. Certain experiments seem to indicate liquid phase diffusional resistance whereas some indicate batch distillation mode with uniform droplet composition. This puts into doubt the concept of internal motion within the droplet in the presence of convection for different multi - component fuels. A detailed study of the droplet internal motion and transfer processes might resolve this issue.

## REFERENCES

- 1 *Annual Energy Review*, 2002, Energy Information Administration, U.S. Department of Energy, Washington D.C.
- 2 ANNAMALAI K, RYAN W and CHANDRA S. Evaporation of multicomponent drop arrays. *J. Heat Transfer*, August 1993, **115**, 707-716.
- 3 SIRIGNANO W A and LAW C K. Transient heating and liquid phase mass diffusion in fuel droplet vaporization, Evaporation and Combustion of fuels, *ACS Advances in Chemistry Series*, 1978, **166**, 1-26.
- 4 GODSAVE G.A. Studies of the combustion of drops in a fuel spray: the burning of single drops of fuel. Fourth International Symposium on Combustion, Cambridge, Massachusetts, 1953, 818-830.
- 5 SPALDING D.B. The combustion of liquid fuels. Fourth International Symposium on Combustion, Cambridge, Massachusetts, 1953, 847-864.
- 6 WILLIAMS A. Combustion of droplets of liquid fuels: A Review. *Combust. Flame*, 1973, **21**, 1-31.
- 7 LAW C K. Recent advances in droplet vaporization and combustion, *Prog. Energy Combust. Sci.*, 1982, **8**, 171-201.
- 8 LAW C K. Mechanisms of droplet combustion. 2<sup>nd</sup> Colloquium (International) on Drops and Bubbles, Monterey, California, 1982, 39-53.
- 9 KUMAGAI S, SAKAI T and OKAJIMA S. Combustion of free fuel droplets in a freely falling chamber. Thirteenth International Symposium on Combustion, Saltlake City, Utah, 1971, 779-785.
- 10 LAW C K, CHUNG S H and SRINIVASAN N. Gas phase quasi-steadiness and fuel vapor accumulation effects in droplet burning. *Combust. Flame*, 1980, **38**, 173.
- 11 LANDIS R B and MILLS A F. Effects of internal resistance on the vaporization of binary droplets. 5th Int. Heat Transfer Conf., Tokyo, Japan, Paper B7-9, 1974.
- 12 LAW C K. Multicomponent droplet combustion with rapid internal mixing. *Combust. Flame*, 1976, **26**, 219-233.
- 13 WILLIAMS F A. *Combustion Theory*, Benjamin/Cummins, New York, 1985.
- 14 TURNS S R. *An Introduction to Combustion: Concepts and Applications*, McGraw-Hill, Boston, 2000.
- 15 ANNAMALAI K., *Final Draft: Combustion Science and Engineering*, CRC Press, Boca Raton, Florida, 2004.

- 16 LAW C K and LAW H K. A  $d^2$ -law for multicomponent droplet vaporization and combustion. *AIAA J.*, April 1982, **20**(4), 522-527.
- 17 RANDOLPH A L, MAKINO A and LAW C K. Liquid phase diffusional resistance in multicomponent droplet gasification. 21<sup>st</sup> Symposium (International) on Combustion, Munich, Germany, 1986, 601-608.
- 18 GALLANT R W. Physical Properties of Hydrocarbons, Vol. 1, Gulf Publishing, Houston.
- 19 GALLANT R W. Physical Properties of Hydrocarbons, Vol. 2, Gulf Publishing, Houston.
- 20 GALLANT R W. Physical Properties of Hydrocarbons, Vol. 3, Gulf Publishing, Houston.
21. CHEMnetBASE. Properties of Organic Compounds, <http://www.chemnetbase.com/scripts/docweb.exe>, (accessed from Sep 2003-May 2004).
- 22 BORMAN G L and RAGLAND K W. Combustion Engineering, McGraw Hill, Boston, 1998.
- 23 HAMILTON B. Components of Gasoline, Archive-name: autos/gasoline-faq/part2, <http://www.cs.uu.nl/wais/html/na-dir/autos/gasoline-faq/part2.html>, (accessed on Sep 15, 2003).
- 24 REID R C and SHERWOOD T K. The properties of gases and liquids, McGraw Hill, New York, 1958.
- 25 LAW C K. Internal boiling and superheating in vaporizing multicomponent droplets. *AIChE J.*, 1978, **24**(4), 626-632.
- 26 RA Y and REITZ R D. A model for droplet vaporization for use in gasoline and HCCI engine applications. *Trans. ASME*, April 2004, **126**, 422-428.
- 27 RA Y., Electronic communication, University of Wisconsin, 2004.
- 28 RA Y and REITZ R D. The application of a multicomponent vaporization model to gasoline direct injection engines. *Int J. Engine Res.*, February 2003, **4**(3), 193-218.
- 29 HARSTAD K and BELLAN J. Modeling evaporation of Jet A, JP-7, and RP-1 drops at 1 to 15 bars. *Combust. Flame*, 2004, **137**, 163-177.

## APPENDIX A

### SHVAB-ZELDOVICH (SZ) VARIABLE FOR MULTICOMPONENT FUELS

This appendix presents a derivation for SZ formulation for a fuel system consisting of multiple components. Illustration will be provided for two components. The gas phase conservation equations for the species and thermal enthalpy are written as follows:

$$\nabla \cdot \left( \rho \vec{v} Y_A - \rho D \nabla Y_A \right) = \dot{w}_A''' \quad (\text{A})$$

$$\nabla \cdot \left( \rho \vec{v} Y_B - \rho D \nabla Y_B \right) = \dot{w}_B''' \quad (\text{B})$$

$$\nabla \cdot \left( \rho \vec{v} Y_{O_2} - \rho D \nabla Y_{O_2} \right) = \dot{w}_{O_2,A}''' + \dot{w}_{O_2,B}''' \quad (\text{C})$$

$$\nabla \cdot \left( \rho \vec{v} h_T - \rho D \nabla h_T \right) = -h_{c,A} \dot{w}_A''' - h_{c,B} \dot{w}_B''' \quad (\text{D})$$

where



The SZ variables can be defined based on the coupling between the fuel-oxidizer species and fuel-energy. Equations (A)-(D) can be coupled accordingly after applying the results from the law of stoichiometry given below, for each of the single step reactions involving components A and B.

$$\frac{\dot{w}_A'''}{-1} = \frac{\dot{w}_{O_2,A}'''}{-\nu_{O_2,A}} = \dot{w}_I''' = \frac{\dot{w}_B'''}{-1} = \frac{\dot{w}_{O_2,B}'''}{-\nu_{O_2,B}} = \dot{w}_{II}''' \quad (\text{G})$$

Then Equations (A)-(D) become:

$$\nabla \cdot \left( \rho \vec{v} Y_A - \rho D \nabla Y_A \right) = -\dot{w}_I''' \quad (\text{H})$$

$$\nabla \cdot \left( \rho \vec{v} Y_B - \rho D \nabla Y_B \right) = -\dot{w}_{II}''' \quad (\text{I})$$

$$\nabla \cdot \left( \rho \vec{v} Y_{O_2} - \rho D \nabla Y_{O_2} \right) = -\nu_{O_2,A} \dot{w}_I''' - \nu_{O_2,B} \dot{w}_{II}''' \quad (\text{J})$$

$$\nabla \cdot \left( \rho \vec{v} h_T - \rho D \nabla h_T \right) = h_{c,A} \dot{w}_I''' + h_{c,B} \dot{w}_{II}''' \quad (\text{K})$$

Multiply (H) by  $\nu_{O_2,A}$  and (I)  $\nu_{O_2,B}$ , add the results, then subtract the result from (J). Then:

$$\nabla \cdot \left( \rho \vec{v} \beta_{O_2-A-B} - \rho D \nabla \beta_{O_2-A-B} \right) = 0 \quad (\text{L})$$

where the modified SZ variable is defined as below

$$\beta_{O_2-A-B} = Y_{O_2} - \nu_{O_2,A} Y_A - \nu_{O_2,B} Y_B \quad (\text{M})$$

Similarly multiply (A) by  $h_{c,A}$  and (B) by  $h_{c,B}$ , add them and add the result with Equation (D). Then:

$$\nabla \cdot \left( \rho \vec{v} \beta_{h_T-A-B} - \rho D \nabla \beta_{h_T-A-B} \right) = 0 \quad (\text{N})$$

where

$$\beta_{h_T-A-B} = h_T + h_{c,A} Y_A + h_{c,B} Y_B \quad (\text{O})$$

Equation (K) can be rewritten as:

$$\nabla \cdot \left( \rho \vec{v} h_T - \rho D \nabla h_T \right) = h_{c,O_2} \nu_{O_2,A} \dot{w}_I''' + h_{c,O_2} \nu_{O_2,B} \dot{w}_{II}''' \quad (\text{P})$$

The heating values based on stoichiometric oxygen are approximately constant for most hydrocarbons, i.e.  $h_{C,O_2} = \frac{h_{C,A}}{\nu_{O_2,A}} \approx \frac{h_{C,B}}{\nu_{O_2,B}}$ . Multiply (J) by  $h_{C,O_2}$  and add with (P). Then:

$$\nabla \cdot \left( \rho \vec{v} \beta_{h_T - O_2} - \rho D \nabla \beta_{h_T - O_2} \right) = 0 \quad (Q)$$

where

$$\beta_{h_T - O_2} = \frac{h_T}{h_{C,O_2}} + Y_{O_2} \quad (R)$$

This variable is used to determine the approximate burn rate of a multicomponent fuel. The procedure to determine the approximate solution is described in Appendix B. Generalizing for multiple components and replacing A, B... by 1,2,3 etc. and using the continuity equation

$$\nabla \cdot \rho \vec{v} = 0 :$$

$$\nabla \cdot \left( \rho \vec{v} \beta - \rho D \nabla \beta \right) = 0 \quad (S)$$

$$\beta_{O_2-1-2\dots} = Y_{O_2} - \sum_{k=1}^k \nu_{O_2,k} Y_k \quad (T)$$

$$\beta_{h_T-1-2\dots} = h_T + \sum_{k=1}^k h_{C,k} Y_k \quad (U)$$

$$\beta_{h_T - O_2} = \frac{h_T}{h_{C,O_2}} + Y_{O_2} \quad (V)$$

where

$$h_{C,O_2} = \frac{h_{C,1}}{\nu_{O_2,1}} \approx \frac{h_{C,2}}{\nu_{O_2,2}} \dots \quad (W)$$



## APPENDIX B

### APPROXIMATE SOLUTION TO DETERMINE DROPLET BURN RATE

Equation (S) of Appendix A for a spherical coordinate system is written as:

$$\rho v r^2 \frac{d\beta}{dr} = \frac{1}{r^2} \frac{d}{dr} (r^2 \rho D \frac{d\beta}{dr}) \quad (\text{A})$$

which is similar to the conventional conservation equation for a single component drop.

The solution of the modified SZ Equation (A) is given by

$$\frac{\beta(\xi) - \beta(\infty)}{\beta(w) - \beta(\infty)} = \frac{1 - e^{-\xi}}{1 - e^{-\xi_w}} \quad (\text{B})$$

The approximate burn rate is obtained by applying the interface energy and species boundary conditions (Annamalai<sup>15</sup>) and coupling them as shown below. The interface energy conservation is given as

$$\left( \frac{\partial h_T}{\partial \xi} \right)_w = -(L_A \epsilon_A + L_B \epsilon_B) \quad (\text{C})$$

The interface species boundary condition is given as

$$\left( \frac{\partial Y_i}{\partial \xi} \right)_w + Y_{i,w} = \epsilon_i, \quad i=A, B, \dots \quad (\text{D})$$

$$\left( \frac{\partial Y_{O_2}}{\partial \xi} \right)_w + Y_{O_2,w} = 0 \quad (\text{E})$$

Equation (D) is expanded for the two fuel components A and B and the corresponding equations multiplied by the heat (enthalpy) of combustion and coupled with Equation (C) to get the following condition:

$$\left( \frac{\partial \beta_{h_T-A-B}}{\partial \xi} \right)_w + (\beta_{h_T-A-B})_w = -L_{multi} + h_{c,multi} \quad (\text{F})$$

Here  $L_{multi}$  is defined as  $(L_A \varepsilon_A + L_B \varepsilon_B)$  and  $h_{c,multi}$  is defined as  $(h_{c,A} \varepsilon_A + h_{c,B} \varepsilon_B)$  and the right hand side in Equation (F) is designated as  $F$ . Differentiating Equation (A) with  $\xi$ , evaluating at  $\xi = \xi_w$  and using the result in Equation (F):

$$\xi_w = \ln \left( 1 + \frac{\beta(w) - \beta(\infty)}{F - \beta(w)} \right) \quad (G)$$

Similarly “F” can be obtained for other modified SZ variables. Table below tabulates the results.

$\beta$	$F$
$\beta_{h_T-A-B}$	$-L_{multi} + h_{c,multi}$
$\beta_{h_T-O_2}$	$-L_{multi} / h_{c,O_2}$
$\beta_{O_2-A-B}$	$v_{O_2,avg}$

With  $\beta_{h_T-O_2}$ ,  $F = -L_{multi} / h_{c,O_2}$ , the burn rate expression is obtained as:

$$\xi_w = \ln \left( 1 + \frac{Y_{o_2,\infty} + \frac{h_{T,\infty}}{h_{c,o_2}}}{\frac{L_{multi}}{h_{c,o_2}}} \right) \quad (H)$$

Equation (H) is the expression for the burn rate of a multicomponent fuel based on which other combustion parameters can be evaluated. Note that  $L_{multi}$  is still unknown since it depends upon flux ratios. Appendix C describes the procedure.

**APPENDIX C**

**RELATION BETWEEN SURFACE FUEL VAPOR MASS FRACTION AND  
FLUX RATIOS**

The relationship between the surface fuel vapor mass fraction and the fuel species flux ratios is essential to evaluate the flux ratios, which in turn determines the burn rate. The relationship is established starting from the solution for the species equation. In general, the solution for the species equation (say species A) is given by:

$$Y_A(\xi) = C_1 + C_2 e^{-\xi} \quad (\text{A})$$

It can be easily shown that  $\frac{\mathcal{E}_{A,w}}{Y_{A,w}} = \frac{\mathcal{E}_{B,w}}{Y_{B,w}} = \dots = C$  as long as diffusivities of A,B,...are all equal to each other. Equation (A) can be applied between  $0 < \xi < \xi_w$  for pure evaporation. For combustion case Equation (A) is applicable between  $\xi_w < \xi < \xi_f$  where flame is assumed to be located when  $\beta_{O_2-A-B} = 0$ . Utilizing the boundary conditions that  $Y_A(\xi_w) = Y_{A,w}$  and  $Y_A(\xi_f) = 0$ , the equation is solved to yield the following result:

$$Y_A(\xi) = Y_{A,w} \frac{(e^{-\xi} - e^{-\xi_f})}{(e^{-\xi_w} - e^{-\xi_f})} \quad (\text{B})$$

Similarly for species B,

$$Y_B(\xi) = Y_{B,w} \frac{(e^{-\xi} - e^{-\xi_f})}{(e^{-\xi_w} - e^{-\xi_f})} \quad (\text{C})$$

Substituting these equations in the species boundary condition given by Equation (D) of Appendix B, the following expressions can be derived for the individual species flux ratios:

$$\mathcal{E}_A = -Y_{A,W} \frac{(e^{-\xi_f})}{(e^{-\xi_w} - e^{-\xi_f})} \quad (\text{D})$$

$$\mathcal{E}_B = -Y_{B,W} \frac{(e^{-\xi_f})}{(e^{-\xi_w} - e^{-\xi_f})} \quad (\text{E})$$

Dividing (D) by (E) gives the following expression:

$$\frac{\mathcal{E}_A}{Y_{A,w}} = \frac{\mathcal{E}_B}{Y_{B,w}} = c \quad (\text{F})$$

which is similar to the result for pure evaporation. Generalizing Equation (F):

$$\frac{\mathcal{E}_A}{Y_{A,w}} = \frac{\mathcal{E}_B}{Y_{B,w}} = \frac{\mathcal{E}_C}{Y_{C,w}} = \dots = c \quad (\text{G})$$

Then:

$$\mathcal{E}_A + \mathcal{E}_B + \dots = c(Y_{A,w} + Y_{B,w} + \dots) = c(1 - Y_{I,w}) \quad (\text{H})$$

Summing the flux ratios of all the  $i$  species and using equation (H):

$$\frac{1}{(1 - Y_{I,w})} = \frac{\mathcal{E}_i}{Y_{i,w}}, i=A,B,C\dots \quad (\text{I})$$

Equation (I) establishes a simple relationship between the vapor species surface mass fractions and flux ratios. The flux ratio evaluated from this is then used to estimate the burn rate.

## APPENDIX D

### ESTIMATING FLAME RADIUS AND FLAME TEMPERATURE

An expression for the flame radius can be derived by applying suitable SZ variable to the solution of the modified SZ Equation (S) given in Appendix A. Using the SZ variable given by Equation (M) of Appendix A, the solution of equation (S) simplifies to:

$$\frac{-\beta_{\infty}}{\beta_w - \beta_{\infty}} = \frac{1 - e^{-\xi_f}}{1 - e^{-\xi_w}} \quad (\text{A})$$

Where  $\beta$  could be  $\beta_{h_t-O_2}$  or  $\beta_{O_2-A-B}$ . Using the expression that  $\xi_f = \frac{\dot{m}}{4\pi\rho D r_f}$

and  $\xi_w = \frac{\dot{m}}{4\pi\rho D a} = \ln(1 + B)$ , we get the following relationship between  $\xi$  and  $\xi_w$ :

$$\xi_f = \xi_w \frac{a}{r_f} = \ln(1 + B) \frac{a}{r_f} \quad (\text{B})$$

Combining Equations (A) and (B), the expression for flame location is obtained as:

$$\xi_f = -\ln\left(\frac{B}{1+B}\right)\left(\frac{\beta_{\infty}}{\beta_w - \beta_{\infty}}\right) + 1 \quad (\text{C})$$

Similarly an expression for the flame temperature can be obtained using the SZ variable given by Equation (R) of Appendix A and applying it to the general solution of the modified SZ equation.

Solving:

$$T_f = T_w + \frac{\beta_{\infty} h_{C,O_2}}{c_p} \left(1 - \frac{1 - e^{-\xi_f}}{1 - e^{-\xi_w}}\right) \quad (\text{D})$$

where

$$\beta_{\infty} = \beta_{h_t-O_2,\infty} = \frac{c_{p,g}(T_{\infty} - T_w)}{h_{C,O_2}} + Y_{O_2,\infty} \quad (\text{E})$$

## VITA

Kannan Vittilapuram Subramanian was born in the southern suburb of Chennai in South India on 15<sup>th</sup> of May 1980 to Mr. Subramanian and Mrs. Padmini Subramanian. Kannan spent the first few years of his childhood in Madurai where he completed first grade. He later moved to Chennai and attended Hindu Senior Secondary School till tenth grade. Kannan completed his higher secondary education at Vana Vani Matriculation Higher Secondary School in May 1997. Kannan then completed a dual degree program, majoring in Biological Sciences and Mechanical Engineering from Birla Institute of Technology and Science, Pilani in July 2002. Kannan began his graduate studies at Texas A&M University in fall 2002 and joined the combustion group, advised by Dr.Kalyan Annamalai. Kannan received his Masters in Mechanical Engineering in December 2004. Kannan hopes to work and gain experience in the field of emission control for a year or two before embarking on the journey to his ultimate ambition of becoming a research faculty. Kannan's permanent address is:

Kannan Vittilapuram Subramanian

No 6, 2<sup>nd</sup> East Street

Kamaraj Nagar

Tiruvanmiyur

Chennai – 600041

Tamil Nadu

India